Cell Reports

Prolonged epigenomic and synaptic plasticity alterations following single exposure to a psychedelic in mice

Graphical abstract

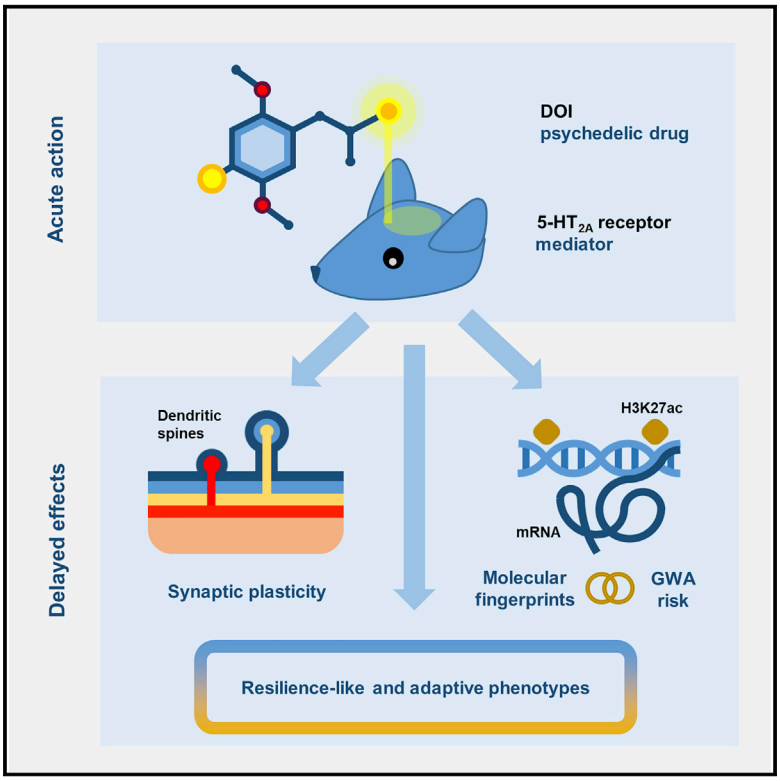

Highlights

- Exposure to the psychedelic drug DOI results in enduring molecular adaptations
- Post-acute DOI unveils phenotypes akin to antidepressant adaptations
- Concurrent occurrence of synaptic plasticity mediated via 5-HT_{2A}R

Authors

Mario de la Fuente Revenga, Bohan Zhu, Christopher A. Guevara, ..., George W. Huntley, Chang Lu, Javier González-Maeso

Correspondence

changlu@vt.edu (C.L.), javier.maeso@vcuhealth.org (J.G.-M.)

In brief

de la Fuente Revenga et al. characterize in-depth molecular changes and behavioral adaptations following exposure to the psychedelic drug DOI. Their findings provide a molecular framework to understand the lingering effects of psychedelics in synaptic plasticity and rodent models of depression.

de la Fuente Revenga et al., 2021, Cell Reports *37*, 109836
October 19, 2021
https://doi.org/10.1016/j.celrep.2021.109836

Cell Reports

CellPress
OPEN ACCESS

Report

Prolonged epigenomic and synaptic plasticity alterations following single exposure to a psychedelic in mice

Mario de la Fuente Revenga,[1,2] Bohan Zhu,[3,7] Christopher A. Guevara,[4,7] Lynette B. Naler,[3] Justin M. Saunders,[1] Zirui Zhou,[3] Rudy Toneatti,[1] Salvador Sierra,[1] Jennifer T. Wolstenholme,[5] Patrick M. Beardsley,[5,6] George W. Huntley,[4] Chang Lu,[3,*] and Javier González-Maeso[1,8,*]

[1]Department of Physiology and Biophysics, Virginia Commonwealth University School of Medicine, Richmond, VA 23298, USA
[2]Virginia Institute of Psychiatric and Behavioral Genetics, Virginia Commonwealth University, Richmond, VA 23298, USA
[3]Department of Chemical Engineering, Virginia Tech, Blacksburg, VA 24061, USA
[4]Nash Family Department of Neuroscience and Friedman Brain Institute, Icahn School of Medicine at Mount Sinai, New York, NY 10029, USA
[5]Department of Pharmacology and Toxicology, Virginia Commonwealth University School of Medicine, Richmond, VA 23298, USA
[6]Center for Biomarker Research and Precision Medicine, Virginia Commonwealth University, Richmond, VA 23298, USA
[7]These authors contributed equally
[8]Lead contact
*Correspondence: changlu@vt.edu (C.L.), javier.maeso@vcuhealth.org (J.G.-M.)
https://doi.org/10.1016/j.celrep.2021.109836

SUMMARY

Clinical evidence suggests that rapid and sustained antidepressant action can be attained with a single exposure to psychedelics. However, the biological substrates and key mediators of psychedelics' enduring action remain unknown. Here, we show that a single administration of the psychedelic DOI produces fast-acting effects on frontal cortex dendritic spine structure and acceleration of fear extinction via the 5-HT_{2A} receptor. Additionally, a single dose of DOI leads to changes in chromatin organization, particularly at enhancer regions of genes involved in synaptic assembly that stretch for days after the psychedelic exposure. These DOI-induced alterations in the neuronal epigenome overlap with genetic loci associated with schizophrenia, depression, and attention deficit hyperactivity disorder. Together, these data support that epigenomic-driven changes in synaptic plasticity sustain psychedelics' long-lasting antidepressant action but also warn about potential substrate overlap with genetic risks for certain psychiatric conditions.

INTRODUCTION

Psychiatric conditions including depression, anxiety, and stressor-related disorders affect the life of millions of individuals worldwide (Kessler et al., 2003; Krishnan and Nestler, 2008). All currently available medications, including monoamine reuptake-based antidepressants such as fluoxetine, paroxetine, and citalopram require several weeks to months for the clinically relevant improvements to occur, and there is a high proportion of patients taking standard pharmacotherapies who remain treatment resistant (Duman and Aghajanian, 2012). In addition, these pharmacological interventions are often accompanied by undesirable side effects (Insel and Wang, 2009). There is therefore an urgent need for better antidepressant treatments, with a faster onset of action, which will also offer relief to patients who do not respond to classic antidepressants.

Psychedelics, which can be classified into two main groups: phenethylamines such as mescaline and the substituted amphetamine 1-(2,5-dimethoxy-4-iodophenyl)-2-aminopropane (DOI) and tryptamines such as psilocybin and lysergic acid diethylamide (LSD), are psychoactive compounds that profoundly affect various mental domains, particularly sensory perception and thought processes (Glennon, 1994). Most of the previous preclinical and human neuroimaging studies focused their efforts on the effects that occur within minutes to hours after psychedelic administration, with the aim of elucidating the molecular and neural circuit mechanisms responsible for their psychotic-like states (Hanks and González-Maeso, 2013; Nichols, 2016). However, recent pilot clinical trials suggest that psychedelics may represent a promising long-lasting treatment for patients with depression and other psychiatric conditions (Carhart-Harris et al., 2016; Griffiths et al., 2016; Davis et al., 2021; Carhart-Harris et al., 2021). As an example, people with cancer demonstrated rapid increases in positive affect after psilocybin administration, with 60%–85% showing long-term improvements in anxiety and depression measures at a 6.5-month follow-up (Griffiths et al., 2016). Despite these striking effects, their acute psychotic symptoms and drug abuse potential preclude the routine use of psilocybin and other psychedelics in daily clinical practice. Therefore, there is a clear need for basic and translational research focused on understanding the molecular mechanisms mediating the clinical effectiveness of psychedelics—with the ultimate goal of developing safer, more effective, and non-psychedelic treatment strategies.

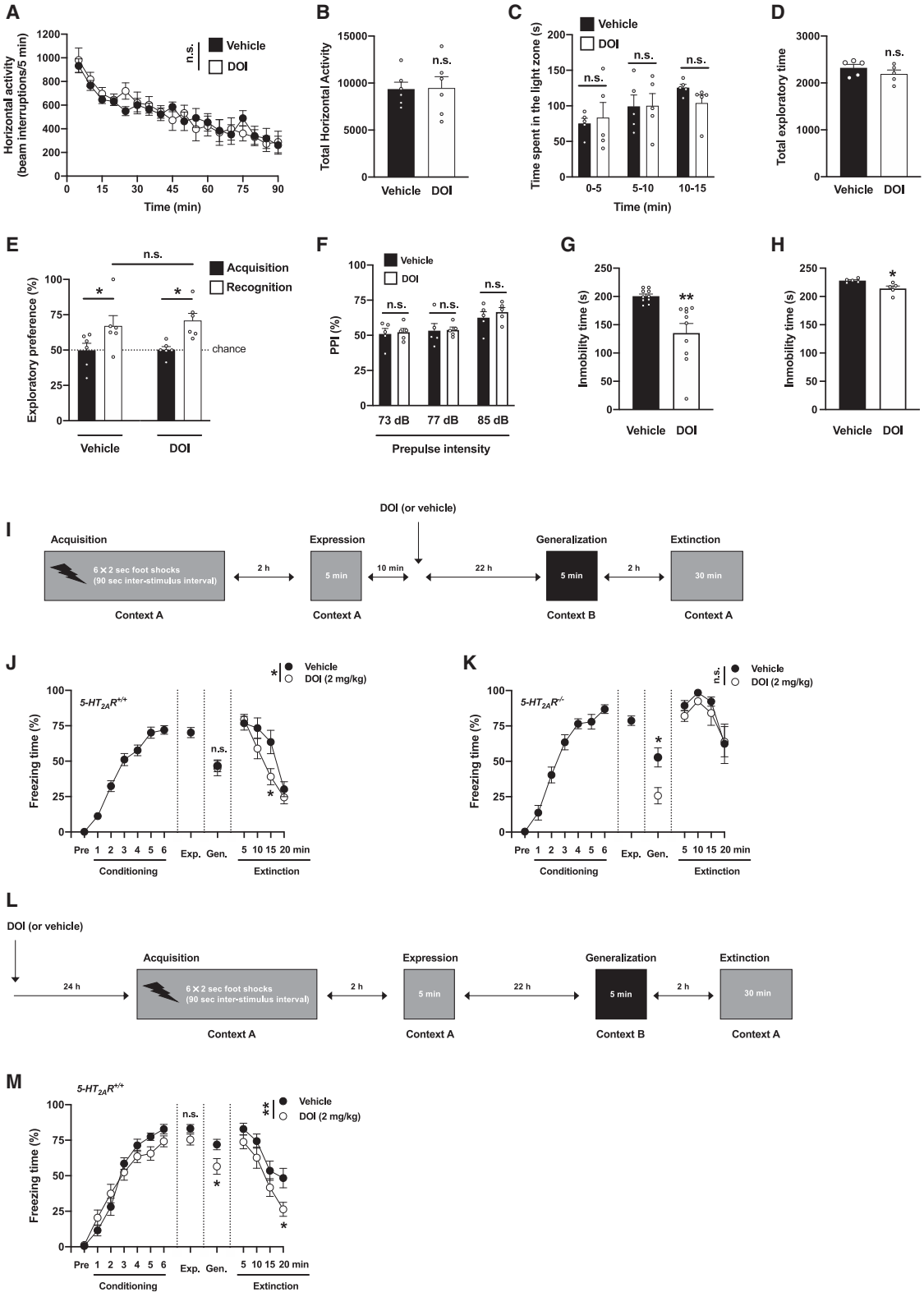

(legend on next page)

Preclinical assays in rodent models have evaluated the effects of psychedelics as rapid-acting antidepressant medications. Notably, it has been suggested that a single administration of psilocybin or LSD produces long-lasting (for 5 weeks post-administration) antidepressant-like effects in rats within models of behavioral despair or passivity such as the forced swim test (Hibicke et al., 2020). Additionally, it has been reported that a single dose of psychedelics such as 4-bromo-3,6-dimethoxybenzocyclobuten-1-yl)methylamine (TCB-2) and *N,N*-dimethyltryptamine (DMT) facilitates the extinction of cued fear memory in mice (Zhang et al., 2013) and rats (Cameron et al., 2018), respectively. The pharmacological profiles of these drugs are notoriously complex (Ray, 2010), but it is well established that the serotonin 5-HT_{2A} receptor (5-HT_{2A}R) in the frontal cortex is involved in the effects of psychedelics on psychosis-like behavior in mouse (González-Maeso et al., 2007) and humans (Vollenweider et al., 1998). With regard to outcomes relevant to depression, anxiety, and stressor-related disorders, the receptor targets responsible for these benign effects of psychedelics remain largely unexplored.

Here, we aimed to unveil the molecular mechanism responsible for the post-acute effects of the psychedelic phenethylamine DOI using mouse behavior models relevant to depression, anxiety, and stressor-related disorders, as well as its implication in crucial plasticity phenotypes including frontal cortex dendritic spine structure, epigenetic alterations (defined as covalent histone modifications on their amino tails that alter chromatic structure and play an important role in regulating transcription), and associated gene expression.

RESULTS

Psychedelics accelerate fear extinction via 5-HT_{2A}R

To explore the potential role of 5-HT_{2A}R in the post-acute effects of psychedelics on behavior models relevant to anxiety, passivity, cognition, and sensorimotor gating, mice were tested 24 h after administration of the psychedelic yet relatively selective 5-$HT_{2A/2C}$R agonist DOI (Canal and Morgan, 2012), or vehicle—a time point at which DOI is no longer detectable in the mouse brain (de la Fuente Revenga et al., 2019). Locomotor activity in a novel environment, as a model of exploratory behavior (Figures 1A and 1B), and time spent in the light compartment using a dark-light choice test, as a conflict paradigm (Figures 1C and 1D), were similar between DOI-treated and vehicle-treated mice. Novel-object recognition (Figure 1E) and prepulse inhibition of startle (Figure 1F) were also unaffected by DOI treatment. However, immobility time in the forced swim test was reduced in DOI-treated mice as compared to controls (Figure 1G)—the trend for reduction in immobility time was also evident 7 days after DOI administration (Figure 1H). These findings indicate that a single dose of DOI reduces behavioral despair or passivity as a model of depression at least 24 h after its administration, whereas behaviors in models of anxiety, recognition memory, and sensorimotor gating remain unchanged.

Fear and anxiety are adaptive defensive behaviors that are mediated by different neural substrates (Tovote et al., 2015). To test whether DOI affects contextual fear conditioning and extinction, as well as the role of 5-HT_{2A}R-dependent signaling in these effects, *5-HT$_{2A}$R$^{+/+}$* and *5-HT$_{2A}$R$^{-/-}$* mice were tested in a paradigm of fear acquisition (context A) and expression (context A). After this, mice were randomly separated into two groups that received a single dose of DOI or vehicle. The day after, DOI- and vehicle-treated groups were tested for fear generalization (context B) and context fear extinction (context A) (Figure 1I). Our data show that there is a modest yet statistically significant increase in fear during fear acquisition in *5-HT$_{2A}$R$^{-/-}$* mice as compared to *5-HT$_{2A}$R$^{+/+}$* controls (Figure S1), whereas no differences were observed during the fear expression session (Figure S1). Administration of DOI had no effect on fear generalization in *5-HT$_{2A}$R$^{+/+}$* mice but reduced freezing time during the generalization session in *5-HT$_{2A}$R$^{-/-}$* littermates (Figures 1J and 1K). Fear extinction was significantly reduced in vehicle-treated *5-HT$_{2A}$R$^{-/-}$* mice as compared to vehicle-treated *5-HT$_{2A}$R$^{+/+}$* controls (Figure S1). Additionally, *5-HT$_{2A}$R$^{+/+}$* mice that had previously received a single dose of DOI showed faster development of contextual fear extinction as exemplified by the progressive reduction in freezing time compared to vehicle-treated animals (Figures 1J and 1K)—an effect that was not observed in *5-HT$_{2A}$R$^{-/-}$* littermates (Figures 1J

Figure 1. Post-acute effects of DOI on passivity and fear extinction

(A–H) Behavior was tested 24 h (A-G) or 7 days (H) after a single injection (i.p.) of DOI (2 mg/kg) or vehicle.

(A and B) Lack of effect of DOI on exploratory behavior in an open field (n = 6 mice per group). Time-course (A, $F[1,10] = 0.006$, $p > 0.05$) and total horizontal activity (B, $t_{10} = 0.07$, $p > 0.05$).

(C and D) Lack of effect of DOI on dark-light choice test (n = 5 mice per group). Time (s) spent in the light zone (C, $F[1,8] = 0.08$, $p > 0.05$) and total exploratory time during the 15-min test (D, $t_8 = 1.14$, $p > 0.05$).

(E) Lack of effect of DOI on the novel-object recognition test (n = 6 mice per group, acquisition versus recognition, $F[1,20] = 13.06$, $p < 0.01$; vehicle versus DOI, $F[1,20] = 0.16$, $p > 0.05$).

(F) Lack of effect of DOI on the PPI of startle (n = 5 mice per group, $F[1,24] = 0.41$, $p > 0.05$).

(G) Reduction of immobility time (s) during the last 4 min of the 6-min forced swimming test (10 mice per group, $t_{18} = 3.80$; $p < 0.01$).

(H) Reduction of immobility time (s) during the last 4 min of the 6-min forced swimming test (5 mice per group, $t_8 = 2.96$; $p < 0.05$).

(I–K) Effect of DOI on contextual fear extinction in *5-HT$_{2A}$R$^{+/+}$* (J) and *5-HT$_{2A}$R$^{-/-}$* (K) mice. Timeline of the experimental design (I). Fear conditioning (J, n = 26 mice, $F[6, 175] = 73.69$, $p < 0.001$; K, n = 12 mice, $F[6, 77] = 58.76$, $p < 0.001$), generalization (J, n = 11–15 mice per group, $t_{24} = 0.24$, $p > 0.05$; K, n = 6 mice per group, $t_{10} = 3.04$, $p < 0.05$), extinction (J, n = 11–15 mice per group, $F[1, 96] = 5.51$, $p < 0.05$; K, n = 6 mice per group, $F[1, 40] = 2.29$, $p > 0.05$).

(L and M) Effect of DOI on fear acquisition. Timeline of the experimental design (L). Fear conditioning (n = 14-15 mice per group; conditioning, $F[6,189] = 95.86$, $p < 0.001$; vehicle versus DOI, $F[1,189] = 0.91$, $p > 0.05$), expression (n = 14-15 mice per group, $t_{27} = 1.61$, $p > 0.05$), generalization (n = 14-15 mice per group, $t_{27} = 2.34$, $p < 0.05$), extinction (n = 14-15 mice per group; extinction, $F[3,104] = 20.17$, $p < 0.001$; vehicle versus DOI, $F[1,104] = 10.65$, $p < 0.01$) (M).

Statistical analysis was performed using two-way repeated-measures ANOVA (A), two-way ANOVA with Sidak's multiple comparison test (C, E, F, J, K, and M), or Student's t test (B, D, G, H, J, K, and M). *$p < 0.05$, **$p < 0.01$, ***$p < 0.001$, n.s., not significant. Error bars represent SEM.

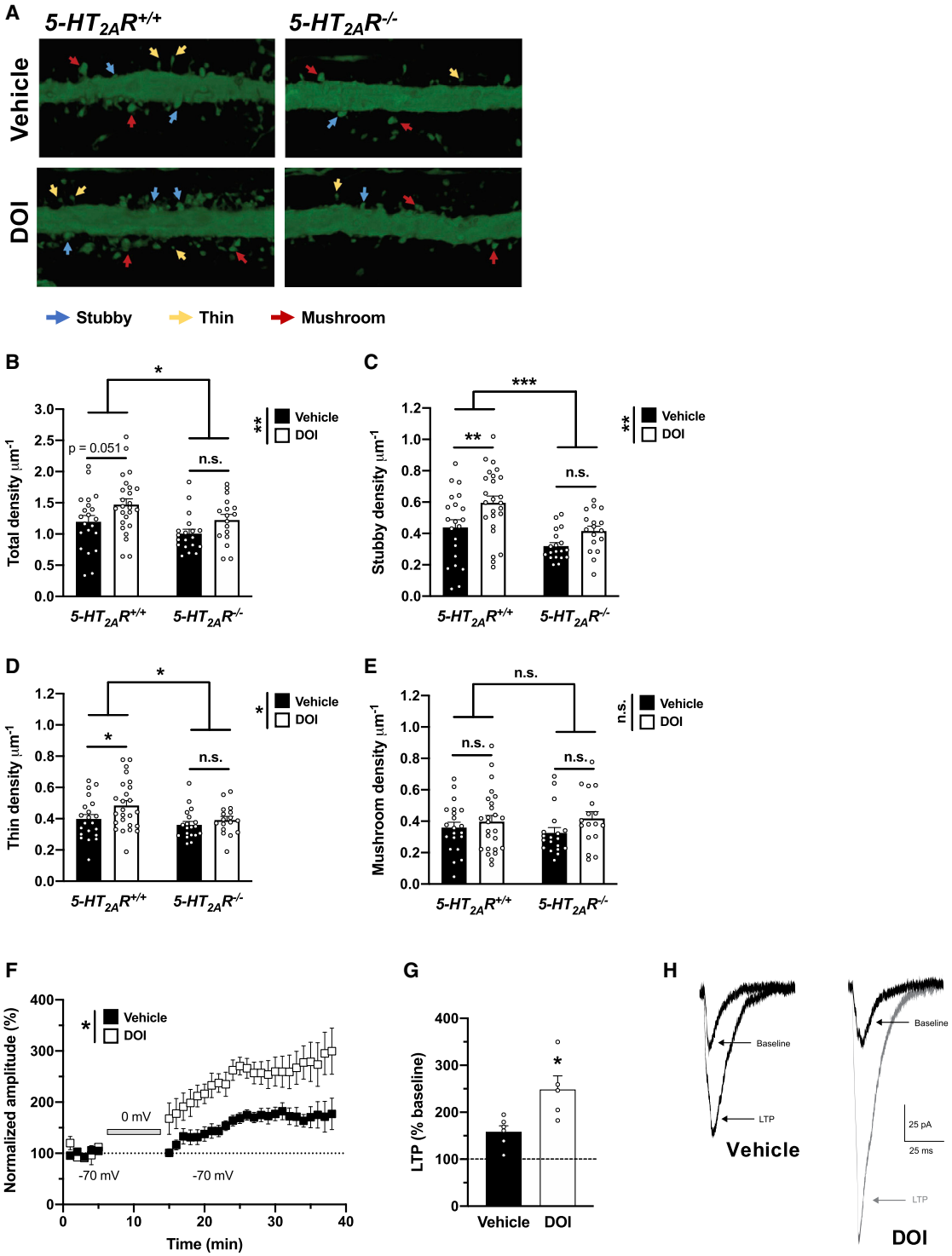

Figure 2. Post-acute effects of DOI on frontal cortex synaptic plasticity

(A–E) Effect of DOI on synaptic structural elements in the frontal cortex of 5-$HT_{2A}R^{+/+}$ and 5-$HT_{2A}R^{-/-}$ mice (n = 17-25 dendrites from independent neurons from both hemispheres in 3–4 mice per group). Samples were collected 24 h after a single injection (i.p.) of DOI (2 mg/kg) or vehicle. Representative three-dimensional reconstructions of AAV-injected cortical dendritic segments (A). Total (B), 5-$HT_{2A}R^{+/+}$ versus 5-$HT_{2A}R^{-/-}$ mice, $F[1,78] = 5.72$, $p < 0.05$; vehicle versus DOI, $F[1,78] = 7.31$, $p < 0.01$), stubby (C), 5-$HT_{2A}R^{+/+}$ versus 5-$HT_{2A}R^{-/-}$ mice, $F[1,78] = 13.56$, $p < 0.001$; vehicle versus DOI, $F[1,78] = 9.65$, $p < 0.01$), thin (D), 5-$HT_{2A}R^{+/+}$ versus 5-$HT_{2A}R^{-/-}$ mice, $F[1,78] = 5.27$, $p < 0.05$; vehicle versus DOI, $F[1,78] = 4.28$, $p < 0.05$), mushroom (E), 5-$HT_{2A}R^{+/+}$ versus 5-$HT_{2A}R^{-/-}$ mice, $F[1,78] = 0.03$, $p > 0.05$; vehicle versus DOI, $F[1,78] = 2.90$, $p > 0.05$).

(legend continued on next page)

and 1K). To test whether psychedelics affect fear acquisition, a different cohort of *5-HT$_{2A}$R$^{+/+}$* mice was subjected to a similar paradigm of fear acquisition, expression, generalization, and extinction but with DOI or vehicle being administered 24 h before the fear-acquisition protocol (Figure 1L). Our data show that DOI did not affect fear acquisition or fear expression, whereas it reduced freezing time during the fear generalization and context fear extinction sessions (Figure 1M)—suggesting that the effects of DOI on associative learning relevant to contextual fear extinction may linger beyond the 24 h after drug administration.

Psychedelics enhance cortical dendritic density via 5-HT$_{2A}$R

Structural and functional modification of dendritic spines are central to brain plasticity (Spruston, 2008; Koleske, 2013). As a general rule, increased synaptogenesis and functional plasticity are tightly correlated with the size and the shape of a dendritic spine; stubby spines are theorized to be transitional structures that will enlarge, possibly into mature mushroom spines, whereas thin spines are highly dynamic and likely to change in response to activity. Basic and clinical studies demonstrate that depression is associated with reduction of synaptic density in brain regions that regulate anxiety, mood, and fear extinction, including the frontal cortex (Duman and Aghajanian, 2012; Savalia et al., 2021). Typical antidepressants like fluoxetine can reverse these synaptic deficits, albeit with limited efficacy and delayed response. Previous studies convincingly demonstrated that a single dose of psychedelics such as DMT (Ly et al., 2018) or psilocybin (Hesselgrave et al., 2021; Shao et al., 2021) promotes rapid structural plasticity in frontal cortex pyramidal neurons. Although interesting, whether psychedelic-induced activation of 5-HT$_{2A}$R-dependent signaling is necessary for the effects of psychedelics on this particular phenotype remains a topic of intense debate. As an example, some (Ly et al., 2018; Cameron et al., 2021) but not all (Hesselgrave et al., 2021; Shao et al., 2021) of the previous studies suggest that the effect of psychedelics on neural plasticity was prevented by pretreatment with the relative selective 5-HT$_{2A/2C}$R antagonist ketanserin. Here, we measured the effect of a single administration of DOI or vehicle on dendritic spine density in cortical pyramidal neurons in *5-HT$_{2A}$R$^{-/-}$* mice and controls. We targeted pyramidal neurons from frontal cortex of adult mice through the injection of adeno-associated virus (AAV8) encoding enhanced yellow fluorescent protein (eYFP) under the control of the *CaMKIIα* promoter. Using a 3D automated method for quantitative structural spine analysis, our findings suggest a lower spine density in the frontal cortex of vehicle-treated *5-HT$_{2A}$R$^{-/-}$* mice as compared to *5-HT$_{2A}$R$^{+/+}$* controls (Figures 2A and 2B), a phenotype that was primarily driven by a selective decrease of stubby (Figures 2A and 2C) and thin (Figures 2A and 2D), but not mushroom (Figures 2A and 2E), spines. Additionally, a single administration of DOI selectively augmented the density of transitional stubby (Figures 2A and 2C) and dynamic thin (Figures 2A and 2D) spines in CaMKIIα-positive frontal cortex neurons but not mature mushroom spine density (Figures 2A and 2E). This psychedelic-induced synaptic remodeling event required expression of 5-HT$_{2A}$R, as the effect of DOI on dendritic spine structure was not observed in *5-HT$_{2A}$R$^{-/-}$* mice (Figures 2A–2E).

Based on these findings of dendritic spine structural plasticity, we next determined whether DOI also regulates persistent synaptic functional plasticity in frontal cortex pyramidal neurons. In vehicle-treated mice, as expected, pairing layer 4 (L4) stimulation with brief postsynaptic depolarization induced robust long-term potentiation (LTP) in L2/3 neurons that was sustained for 30–40 min until the experiment was terminated (Figures 2F–2H). Notably, a significantly greater magnitude of LTP was evident in DOI-treated mice in comparison with that in vehicle-treated mice over the same time course (Figures 2F–2H), indicating that DOI enhanced synaptic plasticity in L2/3 frontal cortex pyramidal neurons.

Psychedelics lead to long-lasting alterations in frontal cortex epigenomic landscapes

Using classic gene-expression assays such as microarrays, previous studies demonstrated that a single administration of psychedelics including DOI and LSD alters the level of expression of several genes that showed maximal changes at ~60 min—returning to basal level at ~2 h after drug exposure (Nichols and Sanders-Bush, 2002; González-Maeso et al., 2003). Several of the genes showing transient induction upon acute psychedelic administration have previously been implicated in processes related to transcription and chromatin organization. However, these previous transcriptomic studies in bulk tissue samples suffered from lack of cell-type specificity in their profiling. Here, we tested whether a single dose of DOI leads to long-lasting epigenomic and transcriptomic alterations in the frontal cortex using high-resolution, cell-type-specific, and low-input ChIP-seq and RNA-seq measurements. Mice (n = 6 animals for each condition) were injected (i.p.) with vehicle or DOI (Figure S2). In the case of DOI injection, frontal cortex samples were collected at 24 h, 48 h, or 7 days after DOI administration. Histone modification H3K27ac (acetylation of histone H3 at lysine 27) along with the transcriptome were profiled in NeuN-positive (NeuN^{+}) neuronal nuclei isolated from the frontal cortex by fluorescence-activated cell sorting (FACS). We applied microfluidic oscillatory washing ChIP-seq (MOWChIP-seq) (Cao et al., 2015; Zhu et al., 2019) and Smart-seq2 (Picelli et al., 2013; Picelli et al., 2014) to profile H3K27ac and transcriptome, respectively, using the small

(F–H) A single dose (i.p) of DOI (2 mg/kg) significantly enhanced cortical LTP in comparison with saline-injected mice assayed 24-h post-injection. Normalized EPSC amplitudes obtained from whole-cell patch-clamp recordings of L2/3 neurons from either DOI-injected (n = 5 neurons from 5 mice) or vehicle-injected (n = 6 neurons from 5 mice) animals. LTP was induced by a protocol that pairs extracellular presynaptic stimulation of L4 neurons with brief (10 min) postsynaptic depolarization of overlying L2/3 neurons to 0 mV (gray bar). Symbols represent EPSCs averaged by 1-min bins (vehicle versus DOI, $F[1,10] = 9.84$, $p < 0.05$) (F). Average magnitude of LTP (normalized EPSCs recorded over the 15- to 40-min post-induction period) from DOI-treated mice and controls ($t_9 = 3.05$, $p < 0.05$) (G). Representative traces of EPSCs recorded from L2/3 neurons from DOI- or vehicle-treated mice at baseline and following induction of LTP (H).
Statistical analysis was performed using two-way ANOVA with Sidak's multiple comparison test (B–E), two-way repeated-measures ANOVA (F), or Student's t test (G). *p < 0.05, **p < 0.01, ***p < 0.001, n.s., not significant. Error bars represent SEM.

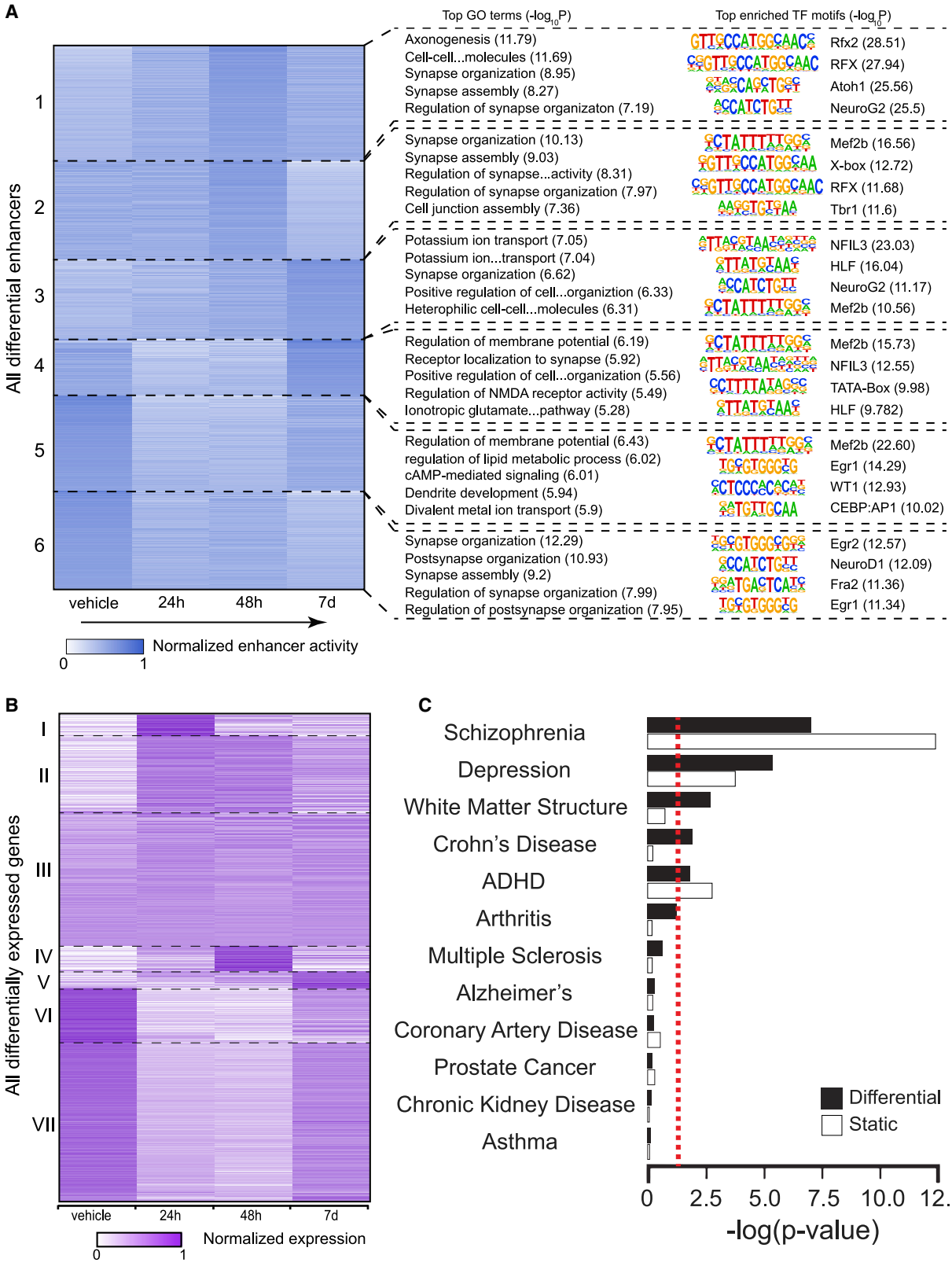

(legend on next page)

quantity of neuronal nuclei yielded from the mouse frontal cortex (Table S1).

Enhancers are highly dynamic epigenomic regulatory elements with known involvement in plasticity and neurodevelopmental processes (Nord and West, 2020). We predicted active enhancers by scanning the H3K27ac^{high} regions that did not intersect with promoters (Cao et al., 2015). H3K27ac mark distinguishes active enhancers from poised and inactive enhancers (Creyghton et al., 2010). H3K27ac and enhancers are also highly differentiating of various brain locations and functions (Ma et al., 2018). We conducted K-means clustering of differential enhancers that showed change from the control (false discovery rate [FDR] <0.05) due to DOI exposure at one or more of the three time points, and examined gene ontology (GO) terms and enriched transcription factor (TF) binding motifs associated with the clusters (Figure 3A). We divided all differential enhancers into 6 clusters with various patterns of variation after DOI injection (Figure 3A). Clusters 1–3 represent enhancers exhibiting eventual increase after DOI administration, while clusters 4–6 show a decrease in DOI-injected mice as compared to vehicle-treated mice. Clusters 1 and 2 show an increase that peaks at 48 h before decreasing at 7 days, while cluster 3 experiences a much slower increase that shows the highest intensity at 7 days. Clusters 4 and 5 have the deepest decrease at 24 h, while enhancer intensity slowly recovers over 48 h and 7 days. Cluster 6 presents an initial decrease at 24 h followed by minor fluctuations at 48 h and 7 days. Interestingly, at least 32.7% of these differential enhancers (clusters 3 and 6) are still in their altered state at 7 days, suggesting long-lasting effects of DOI at the epigenomic level that outlast by several days the presence of the drug in native tissue.

To directly interrogate the functional relevance of these findings, we examined the GO terms and TF motifs associated with each of the clusters (Figure 3A; Tables S2 and S3). Synapse organization and assembly are enriched in all clusters to various degrees (Table S2), consistent with the effects of DOI on structural and synaptic plasticity. The top GO terms enriched in clusters 1 and 2 include axonogenesis, synapse organization, and cell junction assembly. Motifs of several TFs importantly involved in neuronal growth and synaptic plasticity, such as *Mef2B*, *NeuroG2*, and *Atoh1* (Ventéo et al., 2019), are also highly enriched in these clusters. Clusters 4–6, which experience a decrease upon DOI administration, are associated with GO terms related to regulation of glutamate NMDA receptor activity, regulation of membrane potential, and synapse assembly. Enrichment of two zinc finger-containing transcription factors, *Egr1* and *Egr2*, also occurs in clusters 5 and 6. Considering previous findings showing that psychedelics lead to an acute increase in glutamate release as well as augmentation of *Egr1* and *Egr2* transcription in mouse frontal cortex neurons (González-Maeso et al., 2007), these data suggest a compensatory mechanism as a potential explanation for the enhancer intensity decrease observed in clusters 4–6 upon DOI administration. Clusters 3 and 6 represent enhancers with long-lasting (7 days) DOI-dependent increased and decreased activity, respectively. Cluster 3 shows enrichment in GO terms associated with rhythmic processes. This finding, together with *NFIL3*, a TF involved in the mammalian circadian oscillatory mechanism (Mitsui et al., 2001), as the top enriched TF motif in this cluster, shows agreement with long-term effects of psychedelics on sleep-wake cycles. Cluster 6 has synaptic plasticity-related genes heavily enriched (Table S3).

The transcriptomic variations induced by DOI appear to be much more transient than the epigenomic changes (Figure 3B). Based on K-means clustering, only 3.7% (cluster V) of the differentially expressed genes (DEGs, FDR <0.05) present long-term variation (7 days), and only a small number of these genes (n = 574, or 4.2% of the total DEGs) exhibit a pattern of expression that correlates with enhancer dynamics (i.e., with a Spearman's correlation $r > 0.4$ between enhancer intensity and expression level) (Figure S3; Table S4). These results suggest that the long-term effects of the psychedelic DOI are associated with epigenomic regulations of greater magnitude than changes in transcriptomic dynamics.

We then examined the overlap between H3K27ac peaks and single-nucleotide polymorphisms (SNPs) associated with depression, as were reported based on genome-wide association studies (GWAS). Disease-associated variants are known to be generally concentrated in regulatory DNA elements such as enhancers (Maurano et al., 2012). To ascertain whether the overlap was significant, a null distribution was calculated using the set of all SNPs for a specific GWAS dataset. Furthermore, eleven other GWAS sets that are associated with various traits were also analyzed to determine specificity (Figure 3C; Table S5). We separated H3K27ac peaks into differential (i.e., having changes due to DOI exposure) and static (i.e., no change due to DOI exposure) groups and analyzed their overlap with the GWAS sets separately (Figure 3C). Of the 12 GWAS loci datasets, three (schizophrenia, depression, and attention-deficit hyperactivity disorder [ADHD]) had statistically significant overlap ($p < 0.05$) with both differential and static peak groups. Another two GWAS sets (white matter structure, and Crohn disease) showed only significant overlap with the differential H3K27ac peaks, suggesting that epigenomic changes due to DOI exposure altered activity at the GWAS loci associated with the two traits.

We further investigated our RNA-seq data using weighted correlation network analysis (WGCNA) with the goal of detecting

Figure 3. Post-acute effects of DOI on frontal cortex epigenomic and transcriptomic variations

(A) Effect of DOI on time-lapse epigenomic variations in neuronal nuclei of the mouse frontal cortex. K-means clustering of differential enhancers based on normalized H3K27ac signal (n = 3,995; Cluster sizes from top to bottom: 852, 718, 585, 419, 700, and 721). The top-five enriched biological process gene ontology (GO) terms identified by clusterprofiler are listed next to each cluster, and the top four motifs enriched in each cluster are listed next to the GO terms together with their sequences (n = 6 mice per group).

(B) K-means clustering of normalized gene expression (n = 13,605). Cluster sizes from top to bottom: 604, 2,120, 3,748, 708, 497, 1,507, 4,421.

(C) Significance of overlaps between differential and static H3K27ac peaks and NHGRI-EBI GWAS SNP sets. Significance is calculated using a null distribution and is shown as uncorrected –log(p value). The red dotted line denotes $p < 0.05$ cutoff. GWAS sets are ordered according to significance associated with the differential peaks.

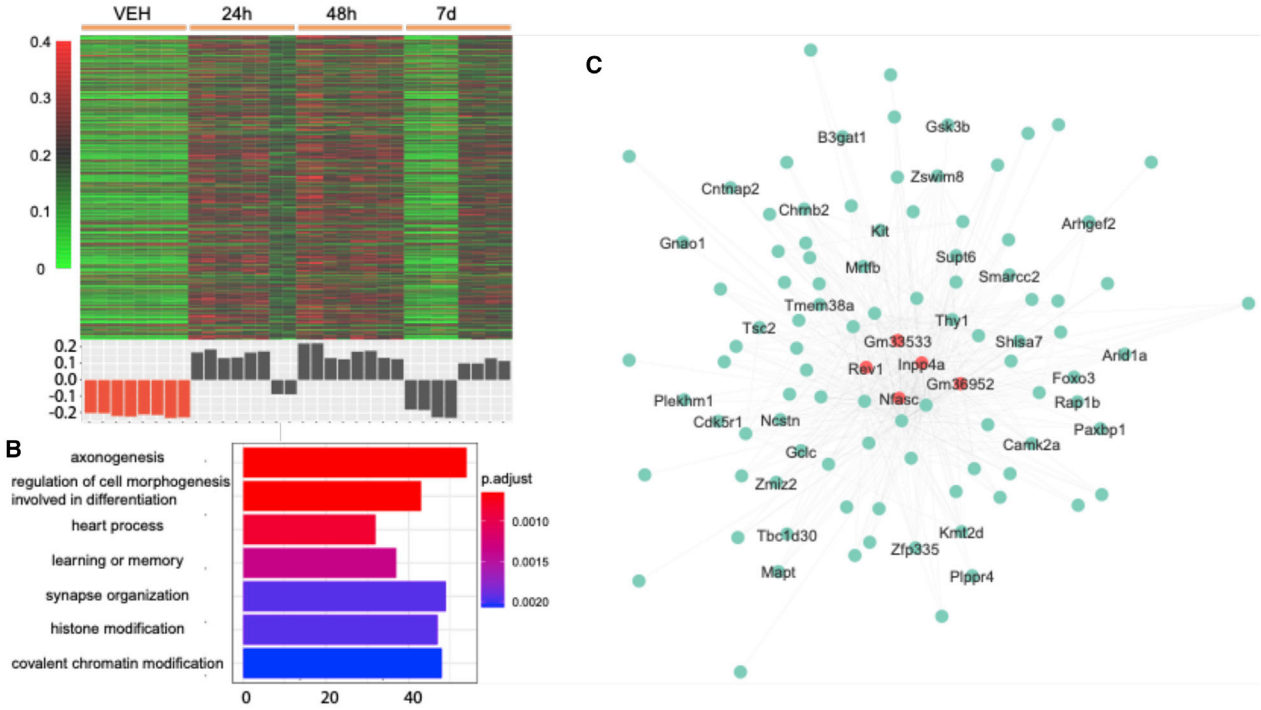

(legend on next page)

co-expression modules with highly correlated genes to associate these modules with sample traits or experimental groups (Langfelder and Horvath, 2008). 14,727 genes with their expression levels throughout all samples in the top 30% were selected, and the generated data matrix was used as the input for WGCNA. After construction of a co-expression network from the matrix, ten modules with densely interconnected genes were detected and the expression pattern in each module was summarized by the module eigengene (Table S6). The eigengene significance was used for assessing correlation between experimental groups and each module. We performed GO analysis on the genes included in these modules and 5 modules (blue, green, turquoise, yellow, and magenta) showed significantly enriched GO terms (Figure 4; Figure S4).

Among all 10 modules, module blue showed the strongest positive correlation with group 48 h and the strongest negative correlation with the control group (Figure S4J). Compared to the control, the eigengene of module blue is overexpressed in both 24 and 48 h groups before decreasing to the control level on 7 days (Figure 4A). GO analysis of this cluster of 1,933 genes leads to terms including: ''axonogenesis'' (p.adjust 6.44×10^{-4}), ''heart process'' (p.adjust 8.32×10^{-4}), ''learning or memory'' (p.adjust 1.35×10^{-3}), and ''histone modification'' (p.adjust 1.95×10^{-3}) (Figure 4B). The GO term ''axonogenesis'' is also identified in the cluster 1 of differential enhancers (Figure 3A). *Inpp4a*, *Nfasc*, and *Cntnap2* are in the top 100 hub genes of module blue (Figure 4C; Table S7). Previous studies suggested that *Inpp4a* may play an important role in the development of epilepsy (Wang et al., 2018). Epileptic seizures have been reported as a result of psychostimulant drug use, although this adverse effect is less common with psychedelics than with other psychostimulants such as cocaine (Zagnoni and Albano, 2002). Loss of function of *Inpp4a* also increases severity of asthma, which may explain the mechanism underlying the effect of DOI preventing allergic asthma in a mouse model (Nau et al., 2015). *Cntnap2* and *Nfasc*, which are genes previously involved in axonal guidance, synaptogenesis and neuron-glial cell interactions (Zonta et al., 2008; McIntyre et al., 2010; Klingseisen et al., 2019) as well as implicated in neurodevelopmental psychiatric conditions such as schizophrenia and autism (Friedman et al., 2008; Peñagarikano and Geschwind, 2012; Rodenas-Cuadrado et al., 2016), were also identified in differential enhancers from clusters 3 and 6 (Figure 3A), respectively.

The eigengene expression in module yellow shows opposite trend of that in module blue (Figure 4D). Among all 10 modules, module yellow is the only one that showed a positive correlation with the control group (Figure S4J). GO biological process enrichment for the genes in module yellow leads to terms including: ''synaptic vesicle recycling'' (p.adjust 0.021), ''drug transport'' (p.adjust 0.021), ''vesicle-mediated transport in synapse'' (p.adjust 0.021), and ''regulation of cation transmembrane transport'' (p.adjust 0.022) (Figure 4E). Interestingly, this module was also enriched with genes related to hypoxia-inducible factor 1 (HIF-1) signaling pathway, including *Slc2a1*, *Eno2* (hub gene), *Gapdh*, *Aldoa*, *Mapk3*, *Pfkl*, and *Pfkm* (hub gene) (Figure 4F; Table S7). Since the HIF-1 pathway is a major modulator of hypoxia stress response pathways (Majmundar et al., 2010), these findings further support the hypothesis the 5-HT_{2A}R modulate the ventilatory response to hypoxia (Anju and Paulose, 2011).

Module magenta's eigengene shows no correlation with any experimental groups (correlation coefficient in the range of −0.12 to 0.05, Figures S4A and S4J). The genes in module magenta are enriched in terms related to inflammatory response and intrinsic apoptotic signaling pathways (Figure S4B). Modules green and turquoise have their eigengenes in a similar pattern as that of module blue (Figures S4D, S4G, and S4J). Their top GO terms were ''synapse organization'' (p.adjust 1.89×10^{-4}) and ''mRNA processing'' (p.adjust $2.61 \times \times 10^{-17}$) (Figures S4E and S4H).

DISCUSSION

Previous observations in rodent models clearly showed that a single administration of psychedelics leads to long-lasting effects on synaptic plasticity and behavior models of depression (Cameron et al., 2018; Ly et al., 2018; Hibicke et al., 2020; Shao et al., 2021). Based on both pharmacological (de la Fuente Revenga et al., 2019) and genetic (González-Maeso et al., 2007) tools, it is clear that the effects of psychedelics on mouse behavior models of human hallucinogenic potential such as head-twitch behavior are mostly 5-HT_{2A}R dependent. However, it remains an open question whether this serotonin receptor is responsible for the manifestation of phenotypes associated with their therapeutic-related effects on preclinical models of neuropsychiatric conditions (Ly et al., 2018; Cameron et al., 2021; Hesselgrave et al., 2021; Shao et al., 2021). In the present study, our data provide direct evidence that the post-acute effects of the phenethylamine psychedelic DOI on mouse frontal cortex dendritic spine structure and contextual fear extinction are 5-HT_{2A}R dependent. Our data also suggest that a single administration of DOI leads to long-lasting alterations in frontal cortex gene expression and chromatin organization that outlast the acute action of this psychedelic and its presence in the organism.

One of the still-open questions in the field is whether the subjective effects of psychedelics are necessary or complementary for their post-acute clinically relevant outcomes in patients with severe psychiatric disorders such as depression (Olson, 2020; Yaden and Griffiths, 2020). Thus, it could be speculated that the fast-acting and long-lasting antidepressant properties induced by psychedelics is a consequence of complex psychological processes, such as waking consciousness, derealization,

Figure 4. Two gene co-expression modules (blue and yellow) associated with administration of DOI

(A and D) Heatmap of normalized gene expression profiles in the co-expression module (top). The module eigengene values across samples in four experimental groups (bottom).

(B and E) Selected top categories from GO enrichment analysis.

(C and F) Visualization of the intramodular connections among the top 100 hub genes in each module. The top 5 genes are in large size and colored orange. The genes involved in the top 15 GO terms are labeled.

and diminished ego functioning (Vollenweider et al., 1998; Schmid et al., 2015). It has also been reported that psilocybin can induce mystical and spiritually significant experiences to which participants attribute increases in well-being (Griffiths et al., 2008). These subjective components of psychedelic drug action appear to be difficult to control with placebo in the clinical setting due to the overwhelming nature of the drug effect. Accordingly, recent studies highlight the role for positive expectancy in predicting positive outcomes following psychedelic microdosing in healthy volunteers and increases in suggestibility under the effect of these drugs (Kaertner et al., 2021). Obviously, these intricate mental experiences, which rely upon subjective reports, would be difficult, perhaps impossible, to model in rodents. However, the recursiveness of the neocortex structure across the mammalian clade and some evolutionarily preserved behaviors inherently linked to constructs relevant to mental health offer an unparalleled platform for characterizing non-subjective effects of psychedelics. Our data in this study, along with previous observations (Jones et al., 2009; Cameron et al., 2018; Ly et al., 2018; Hibicke et al., 2020), suggest that favorable outcomes of psychedelics in processes related to cortical dendritic spine structure and behavior models relevant to depression and stressor-related disorders can be observed in rodents and therefore segregated from uniquely human subjective processes such as attribution of mystical meaning to the psychedelic experience. It is then feasible that quantifiable molecular events and subjective experience concur in the therapeutic benefit of psychedelics in human. Studies like the present utilizing animal models can therefore offer valuable insights on the biological substrate of the equation.

We found that a single administration of the psychedelic DOI leads to a post-acute (24 h after) increase on the density of immature and transitional dendritic spines that included thin and stubby, whereas the density of mature mushroom spines was unaffected. This effect of DOI on frontal cortex dendritic spine structure was not observed in *5-HT$_{2A}$R$^{-/-}$* mice, but it is important to remark that vehicle-injected *5-HT$_{2A}$R$^{-/-}$* mice also showed reduced density of frontal cortex thin and stubby dendritic spine density in the frontal cortex as compared to vehicle-injected *5-HT$_{2A}$R$^{+/+}$* controls. Although further investigation is necessary to unravel the mechanisms underlying this alteration in mice lacking the 5-HT$_{2A}$R, a potential explanation may be related to changes among developmental compensatory pathways also involved in the alterations in fear conditioning and extinction observed in *5-HT$_{2A}$R$^{-/-}$* mice. Additionally, behavioral alterations upon post-acute DOI administration such as reduction in immobility time in the forced-swim test as well as changes in frontal cortex structural plasticity were observed in naive mice. Although interesting, additional investigation will be necessary using behavior models that fall within the current version of the RDoC matrix and paradigms such as early life stress or chronic social defeat in rodents (Bale et al., 2019).

Our findings on the epigenomic and transcriptomic dynamics following DOI administration are significant. There have been no integrative studies of temporal changes in frontal cortex epigenome and transcriptome after psychedelic administration previously. Genome-wide epigenetic changes have long been speculated to be the layer of regulation that integrates both genetic and environmental factors (Gräff and Tsai, 2013; Bastle and Maze, 2019). We show that the epigenetic landscape can be exogenously reshaped by a drug that elicits unequivocal psychedelic effects in humans. At the genomic level, genetic variations in non-coding regions may lead to propensity for depression, schizophrenia, and other psychiatric conditions via long-range chromatin regulation such as enhancer-promoter interaction. In this study, we report that, in contrast to the fairly rapid and transient changes in the transcriptome, a large fraction of epigenetic changes in enhancer regions persist for at least 7 days after DOI administration and potentially constitute the molecular basis for the long-lasting effects. It is worth noting that our findings were established by studying the entire neuronal cell population. Further examination of individual cell types (e.g., excitatory and inhibitory neurons) may yield additional information on the roles of specific neuron types.

We also studied the points of convergence between genetic loci associated with a number of human disorders and the footprint of DOI in the mouse brain epigenome. The peaks of H3K27ac showed significant overlap with GWAS-discovered variants associated with schizophrenia, depression, and ADHD. Although psychedelics have been shown to have fast-acting and long-lasting therapeutic effect on depression (Savalia et al., 2021), their effects on schizophrenia and ADHD remain unknown even when taking into account some overlap between these three psychiatric disorders (Gough and Morrison, 2016; Grace, 2016; Babinski et al., 2020). The acute effects of psychedelics resemble some of the positive symptoms (i.e., hallucinations and delusions) in patients with schizophrenia (Vollenweider et al., 1998; Schmid et al., 2015), and chronic LSD administration alters rat frontal cortex expression of a group of genes relevant to schizophrenia (Martin et al., 2014). Markers linked to white matter structural changes, which have been associated with depression (Liang et al., 2019), were also significantly altered upon DOI administration.

Other than outcomes in the treatment of depression, synaptic plasticity events in diverse parts of the brain have been linked to different adaptive and maladaptive traits. Previous studies have clearly demonstrated that psychoactive drugs of abuse such as cocaine increase dendritic spine density within key components of the brain's reward circuitry, such as the nucleus accumbens (Maze et al., 2010). It has also been reported that the density of immature thin dendritic spines is increased in the frontal cortex of a genetic rat model that exhibits schizophrenia-relevant features (Sánchez-González et al., 2021). Brain regions enriched in 5-HT$_{2A}$R include the frontal cortex, ventral striatum, several thalamic nuclei, and the hypothalamus (Jakab and Goldman-Rakic, 1998; Lopez-Gimenez et al., 2001). Considering our previous findings suggesting that the 5-HT$_{2A}$R in frontal cortex pyramidal neurons is necessary and sufficient for the effects of psychedelics on psychosis-related behavior (González-Maeso et al., 2007), here we focused our efforts on the post-acute effects of the psychedelic DOI in this particular brain region. Although our data provide evidence of long-lasting effects of a single administration of psychedelics on epigenomic landscape within neuronal nuclei in the frontal cortex, additional efforts will be required to establish whether these changes in synaptic plasticity and chromatin rearrangement can be extrapolated to other brain regions relevant to substance abuse, and whether other

cortical and subcortical dendritic structural and epigenetic plasticity events contribute to either clinically beneficial endpoints or, alternatively, unwanted side effects such as drug addiction, psychotic symptoms, or hallucinogen persisting perception disorder.

Our previous work focused on the fundamental paradox that all known psychedelics are 5-HT_{2A}R agonists, but 5-HT_{2A}R agonism is not a sufficient condition for psychedelic action—as exemplified by structurally related drugs such as lisuride or ergotamine that do not exhibit psychedelic activity. We reported that a single dose of psychedelics, such DOI, LSD, or psilocin, induces frontal cortex 5-HT_{2A}R-dependent expression of genes associated with cell morphogenesis, neuron projection, and synapse structure, such as *Egr1*, *Egr2*, *IκBα*, and *N10*. Other genes, such as *c-Fos*, were induced by either psychedelic or non-psychedelic 5-HT_{2A}R agonists (Gonzalez-Maeso et al., 2003, 2007). Our data here support a scheme whereby a single dose of the phenethylamine DOI leads to changes in frontal cortex synaptic plasticity and behavior models of fear extinction. Considering the associative learning processes involved in contextual fear conditioning and extinction, and the effect of DOI on the faster development of the later, it is plausible that activation of 5-HT_{2A}R by this psychedelic accelerates context fear extinction likely in part through alterations in chromatin state at enhancer regions of genes predominantly involved in synapse organization and assembly such as *Mef2B*, *NeuroG2*, and *Atoh1*—a gene network that may be located downstream of the genes showing transient transcription upon acute psychedelic administration. Recent observations have also reported that a putative non-hallucinogenic psychedelic analog referred to as tabernanthalog promotes neural plasticity and reduces rodent behavior models relevant to depression (Cameron et al., 2021). Further work will be needed to unravel the cellular signaling and neural target mechanism that may link psychedelic-induced synaptic plasticity and behavior, as well as the role, if any, of 5-HT_{2A}R in these plasticity-related events induced by non-hallucinogenic 5-HT_{2A}R agonist variants. Similarly, it will be interesting to expand this analysis in future studies to test the extent to which signaling mechanisms unrelated to 5-HT_{2A}R are responsible for the effects of tryptamine psychedelics such as psilocybin on brain plasticity and long-lasting antidepressant-related behavior (Hesselgrave et al., 2021; Shao et al., 2021).

In conclusion, our study highlights the fundamental role of 5-HT_{2A}R in the action of psychedelics and unveils persisting chromatin remodeling events following DOI administration linked to lasting synaptic plasticity and behavioral events. If generalizable to other psychedelics currently in clinical studies, these findings could also facilitate the understanding of psychopharmacological interventions whose mechanisms of action are not fully understood. Last, the overlap of the epigenomic markers of the action of the psychedelic DOI with loci associated with schizophrenia reiterate the need for caution in the use of psychedelics in individuals at risk for psychosis.

STAR★METHODS

Detailed methods are provided in the online version of this paper and include the following:

SUPPLEMENTAL INFORMATION

Supplemental information can be found online at https://doi.org/10.1016/j.celrep.2021.109836.

ACKNOWLEDGMENTS

We thank Jennifer Jimenez and Yashu Sampathkumar for technical assistance with behavior assays. M.d.l.F.R. would like to dedicate this manuscript to the memory of Jordi Riba on the anniversary of his passing away. This work was supported in part by the National Institutes of Health grants R01MH084894, R01MH111940, and P30DA033934 (J.G.-M.), R01GM143940 (C.L.), R01NS107512 (G.W.H.), N01DA-17-8932, and N01DA-19-8949 (P.M.B.), P50AA022537 (J.T.W.), F30MH116550 (J.M.S), T32MH087004 (C.A.G.), and T32MH020030 (M.d.l.F.R.).

AUTHOR CONTRIBUTIONS

M.d.l.F.R., B.Z., C.L. and J.G.-M. designed experiments, analyzed data, and wrote the manuscript. C.L. and J.G.-M. supervised the research and obtained funding. M.d.l.F.R., J.M.S., R.T., and S.S., supervised by J.G.-M., performed behavioral and synaptic structure assays. B.Z., L.B.N., and Z.Z., supervised by C.L., performed ChIP-seq and RNA-seq assays and conducted bioinformatic analysis. C.A.G., supervised by G.W.H., performed electrophysiological studies. J.T.W. and P.M.B. provided advice on behavioral assays and editorial suggestions on early drafts of the report. All authors discussed the results and commented on the manuscript prior to submission for publication consideration.

DECLARATION OF INTERESTS

J.G.-M. has a sponsored research contract with *NeuRistic*, and M.d.l.F.R. has a consulting agreement with *Noetic*. The remaining authors declare that they have no conflict of interest.

Received: March 8, 2021
Revised: July 21, 2021
Accepted: September 24, 2021
Published: October 19, 2021

REFERENCES

Anju, T.R., and Paulose, C.S. (2011). Amelioration of hypoxia-induced striatal 5-HT(2A) receptor, 5-HT transporter and HIF1 alterations by glucose, oxygen and epinephrine in neonatal rats. Neurosci. Lett. *502*, 129–132.

Babinski, D.E., Neely, K.A., Ba, D.M., and Liu, G. (2020). Depression and Suicidal Behavior in Young Adult Men and Women With ADHD: Evidence From Claims Data. J. Clin. Psychiatry *81*, 19m13130.

Bale, T.L., Abel, T., Akil, H., Carlezon, W.A., Jr., Moghaddam, B., Nestler, E.J., Ressler, K.J., and Thompson, S.M. (2019). The critical importance of basic animal research for neuropsychiatric disorders. Neuropsychopharmacology *44*, 1349–1353.

Bastle, R.M., and Maze, I. (2019). Chromatin Regulation in Complex Brain Disorders. Curr. Opin. Behav. Sci. *25*, 57–65.

Benjamini, Y., and Hochberg, Y. (1995). Controlling the False Discovery Rate: A Practical and Powerful Approach to Multiple Testing. J. R. Stat. Soc. B *57*, 289–300.

Cameron, L.P., Benson, C.J., Dunlap, L.E., and Olson, D.E. (2018). Effects of N, N-Dimethyltryptamine on Rat Behaviors Relevant to Anxiety and Depression. ACS Chem Neurosci. *9*, 1582–1590.

Cameron, L.P., Tombari, R.J., Lu, J., Pell, A.J., Hurley, Z.Q., Ehinger, Y., Vargas, M.V., McCarroll, M.N., Taylor, J.C., Myers-Turnbull, D., et al. (2021). A non-hallucinogenic psychedelic analogue with therapeutic potential. Nature *589*, 474–479.

Canal, C.E., and Morgan, D. (2012). Head-twitch response in rodents induced by the hallucinogen 2,5-dimethoxy-4-iodoamphetamine: a comprehensive history, a re-evaluation of mechanisms, and its utility as a model. Drug Test. Anal. *4*, 556–576.

Cao, Z., Chen, C., He, B., Tan, K., and Lu, C. (2015). A microfluidic device for epigenomic profiling using 100 cells. Nat. Methods *12*, 959–962.

Carhart-Harris, R.L., Bolstridge, M., Rucker, J., Day, C.M., Erritzoe, D., Kaelen, M., Bloomfield, M., Rickard, J.A., Forbes, B., Feilding, A., et al. (2016). Psilocybin with psychological support for treatment-resistant depression: an open-label feasibility study. Lancet Psychiatry *3*, 619–627.

Carhart-Harris, R., Giribaldi, B., Watts, R., Baker-Jones, M., Murphy-Beiner, A., Murphy, R., Martell, J., Blemings, A., Erritzoe, D., and Nutt, D.J. (2021). Trial of Psilocybin versus Escitalopram for Depression. N. Engl. J. Med. *384*, 1402–1411.

Creyghton, M.P., Cheng, A.W., Welstead, G.G., Kooistra, T., Carey, B.W., Steine, E.J., Hanna, J., Lodato, M.A., Frampton, G.M., Sharp, P.A., et al. (2010). Histone H3K27ac separates active from poised enhancers and predicts developmental state. Proc. Natl. Acad. Sci. USA *107*, 21931–21936.

Davis, A.K., Barrett, F.S., May, D.G., Cosimano, M.P., Sepeda, N.D., Johnson, M.W., Finan, P.H., and Griffiths, R.R. (2021). Effects of Psilocybin-Assisted Therapy on Major Depressive Disorder: A Randomized Clinical Trial. JAMA Psychiatry *78*, 481–489.

de la Fuente Revenga, M., Ibi, D., Saunders, J.M., Cuddy, T., Ijaz, M.K., Toneatti, R., Kurita, M., Holloway, T., Shen, L., Seto, J., et al. (2018). HDAC2-dependent Antipsychotic-like Effects of Chronic Treatment with the HDAC Inhibitor SAHA in Mice. Neuroscience *388*, 102–117.

de la Fuente Revenga, M., Shin, J.M., Vohra, H.Z., Hideshima, K.S., Schneck, M., Poklis, J.L., and González-Maeso, J. (2019). Fully automated head-twitch detection system for the study of 5-HT_{2A} receptor pharmacology in vivo. Sci. Rep. *9*, 14247.

Duman, R.S., and Aghajanian, G.K. (2012). Synaptic dysfunction in depression: potential therapeutic targets. Science *338*, 68–72.

Friedman, J.I., Vrijenhoek, T., Markx, S., Janssen, I.M., van der Vliet, W.A., Faas, B.H., Knoers, N.V., Cahn, W., Kahn, R.S., Edelmann, L., et al. (2008). CNTNAP2 gene dosage variation is associated with schizophrenia and epilepsy. Mol. Psychiatry *13*, 261–266.

Glennon, R.A. (1994). Classical hallucinogens: an introductory overview. NIDA Res. Monogr. *146*, 4–32.

González-Maeso, J., Yuen, T., Ebersole, B.J., Wurmbach, E., Lira, A., Zhou, M., Weisstaub, N., Hen, R., Gingrich, J.A., and Sealfon, S.C. (2003). Transcriptome fingerprints distinguish hallucinogenic and nonhallucinogenic 5-hydroxytryptamine 2A receptor agonist effects in mouse somatosensory cortex. J. Neurosci. *23*, 8836–8843.

González-Maeso, J., Weisstaub, N.V., Zhou, M., Chan, P., Ivic, L., Ang, R., Lira, A., Bradley-Moore, M., Ge, Y., Zhou, Q., et al. (2007). Hallucinogens recruit specific cortical 5-HT(2A) receptor-mediated signaling pathways to affect behavior. Neuron *53*, 439–452.

Gorkin, D.U., Barozzi, I., Zhao, Y., Zhang, Y., Huang, H., Lee, A.Y., Li, B., Chiou, J., Wildberg, A., Ding, B., et al. (2020). An atlas of dynamic chromatin landscapes in mouse fetal development. Nature *583*, 744–751.

Gough, A., and Morrison, J. (2016). Managing the comorbidity of schizophrenia and ADHD. J. Psychiatry Neurosci. *41*, 150251.

Grace, A.A. (2016). Dysregulation of the dopamine system in the pathophysiology of schizophrenia and depression. Nat. Rev. Neurosci. *17*, 524–532.

Gräff, J., and Tsai, L.H. (2013). Histone acetylation: molecular mnemonics on the chromatin. Nat. Rev. Neurosci. *14*, 97–111.

Griffiths, R., Richards, W., Johnson, M., McCann, U., and Jesse, R. (2008). Mystical-type experiences occasioned by psilocybin mediate the attribution of personal meaning and spiritual significance 14 months later. J. Psychopharmacol. *22*, 621–632.

Griffiths, R.R., Johnson, M.W., Carducci, M.A., Umbricht, A., Richards, W.A., Richards, B.D., Cosimano, M.P., and Klinedinst, M.A. (2016). Psilocybin produces substantial and sustained decreases in depression and anxiety in patients with life-threatening cancer: A randomized double-blind trial. J. Psychopharmacol. *30*, 1181–1197.

Hanks, J.B., and González-Maeso, J. (2013). Animal models of serotonergic psychedelics. ACS Chem. Neurosci. *4*, 33–42.

Heinz, S., Benner, C., Spann, N., Bertolino, E., Lin, Y.C., Laslo, P., Cheng, J.X., Murre, C., Singh, H., and Glass, C.K. (2010). Simple combinations of lineage-determining transcription factors prime cis-regulatory elements required for macrophage and B cell identities. Mol. Cell *38*, 576–589.

Hesselgrave, N., Troppoli, T.A., Wulff, A.B., Cole, A.B., and Thompson, S.M. (2021). Harnessing psilocybin: antidepressant-like behavioral and synaptic actions of psilocybin are independent of 5-HT2R activation in mice. Proc. Natl. Acad. Sci. USA *118*, e2022489118.

Hibicke, M., Landry, A.N., Kramer, H.M., Talman, Z.K., and Nichols, C.D. (2020). Psychedelics, but Not Ketamine, Produce Persistent Antidepressant-like Effects in a Rodent Experimental System for the Study of Depression. ACS Chem. Neurosci. *11*, 864–871.

Hideshima, K.S., Hojati, A., Saunders, J.M., On, D.M., de la Fuente Revenga, M., Shin, J.M., Sanchez-Gonzalez, A., Dunn, C.M., Pais, A.B., Pais, A.C., et al. (2018). Role of mGlu2 in the 5-HT2A receptor-dependent antipsychotic activity of clozapine in mice. Psychopharmacology (Berl) *235*, 3149–3165.

Ibi, D., de la Fuente Revenga, M., Kezunovic, N., Muguruza, C., Saunders, J.M., Gaitonde, S.A., Moreno, J.L., Ijaz, M.K., Santosh, V., Kozlenkov, A., et al. (2017). Antipsychotic-induced Hdac2 transcription via NF-κB leads to synaptic and cognitive side effects. Nat. Neurosci. *20*, 1247–1259.

Insel, T.R., and Wang, P.S. (2009). The STAR*D trial: revealing the need for better treatments. Psychiatr. Serv. *60*, 1466–1467.

Jakab, R.L., and Goldman-Rakic, P.S. (1998). 5-Hydroxytryptamine2A serotonin receptors in the primate cerebral cortex: possible site of action of hallucinogenic and antipsychotic drugs in pyramidal cell apical dendrites. Proc. Natl. Acad. Sci. USA *95*, 735–740.

Jones, K.A., Srivastava, D.P., Allen, J.A., Strachan, R.T., Roth, B.L., and Penzes, P. (2009). Rapid modulation of spine morphology by the 5-HT2A serotonin receptor through kalirin-7 signaling. Proc. Natl. Acad. Sci. USA *106*, 19575–19580.

Kaertner, L.S., Steinborn, M.B., Kettner, H., Spriggs, M.J., Roseman, L., Buchborn, T., Balaet, M., Timmermann, C., Erritzoe, D., and Carhart-Harris, R.L. (2021). Positive expectations predict improved mental-health outcomes linked to psychedelic microdosing. Sci. Rep. *11*, 1941.

Kessler, R.C., Berglund, P., Demler, O., Jin, R., Koretz, D., Merikangas, K.R., Rush, A.J., Walters, E.E., and Wang, P.S.; National Comorbidity Survey Replication (2003). The epidemiology of major depressive disorder: results from the National Comorbidity Survey Replication (NCS-R). JAMA *289*, 3095–3105.

Kim, D., Langmead, B., and Salzberg, S.L. (2015). HISAT: a fast spliced aligner with low memory requirements. Nat. Methods *12*, 357–360.

Klingseisen, A., Ristoiu, A.M., Kegel, L., Sherman, D.L., Rubio-Brotons, M., Almeida, R.G., Koudelka, S., Benito-Kwiecinski, S.K., Poole, R.J., Brophy, P.J., and Lyons, D.A. (2019). Oligodendrocyte Neurofascin Independently Regulates Both Myelin Targeting and Sheath Growth in the CNS. Dev. Cell *51*, 730–744.e6.

Koleske, A.J. (2013). Molecular mechanisms of dendrite stability. Nat. Rev. Neurosci. *14*, 536–550.

Krishnan, V., and Nestler, E.J. (2008). The molecular neurobiology of depression. Nature *455*, 894–902.

Kurita, M., Holloway, T., García-Bea, A., Kozlenkov, A., Friedman, A.K., Moreno, J.L., Heshmati, M., Golden, S.A., Kennedy, P.J., Takahashi, N., et al. (2012). HDAC2 regulates atypical antipsychotic responses through the modulation of mGlu2 promoter activity. Nat. Neurosci. *15*, 1245–1254.

Lake, B.B., Ai, R., Kaeser, G.E., Salathia, N.S., Yung, Y.C., Liu, R., Wildberg, A., Gao, D., Fung, H.L., Chen, S., et al. (2016). Neuronal subtypes and diversity revealed by single-nucleus RNA sequencing of the human brain. Science *352*, 1586–1590.

Langfelder, P., and Horvath, S. (2008). WGCNA: an R package for weighted correlation network analysis. BMC Bioinformatics *9*, 559.

Langmead, B., and Salzberg, S.L. (2012). Fast gapped-read alignment with Bowtie 2. Nat. Methods *9*, 357–359. https://doi.org/10.1038/nmeth.1923.

Li, H., Handsaker, B., Wysoker, A., Fennell, T., Ruan, J., Homer, N., Marth, G., Abecasis, G., and Durbin, R.; 1000 Genome Project Data Processing Subgroup (2009). The Sequence Alignment/Map format and SAMtools. Bioinformatics *25*, 2078–2079.

Liang, S., Wang, Q., Kong, X., Deng, W., Yang, X., Li, X., Zhang, Z., Zhang, J., Zhang, C., Li, X.M., et al. (2019). White Matter Abnormalities in Major Depression Biotypes Identified by Diffusion Tensor Imaging. Neurosci. Bull. *35*, 867–876.

Liao, Y., Smyth, G.K., and Shi, W. (2014). featureCounts: an efficient general purpose program for assigning sequence reads to genomic features. Bioinformatics *30*, 923–930.

López-Giménez, J.F., Vilaró, M.T., Palacios, J.M., and Mengod, G. (2001). Mapping of 5-HT2A receptors and their mRNA in monkey brain: [3H] MDL100,907 autoradiography and in situ hybridization studies. J. Comp. Neurol. *429*, 571–589.

Love, M.I., Huber, W., and Anders, S. (2014). Moderated estimation of fold change and dispersion for RNA-seq data with DESeq2. Genome Biol. *15*, 550.

Ly, C., Greb, A.C., Cameron, L.P., Wong, J.M., Barragan, E.V., Wilson, P.C., Burbach, K.F., Soltanzadeh Zarandi, S., Sood, A., Paddy, M.R., et al. (2018). Psychedelics Promote Structural and Functional Neural Plasticity. Cell Rep. *23*, 3170–3182.

Ma, S., Hsieh, Y.P., Ma, J., and Lu, C. (2018). Low-input and multiplexed microfluidic assay reveals epigenomic variation across cerebellum and prefrontal cortex. Sci. Adv. *4*, eaar8187.

Majmundar, A.J., Wong, W.J., and Simon, M.C. (2010). Hypoxia-inducible factors and the response to hypoxic stress. Mol. Cell *40*, 294–309.

Martin, D.A., Marona-Lewicka, D., Nichols, D.E., and Nichols, C.D. (2014). Chronic LSD alters gene expression profiles in the mPFC relevant to schizophrenia. Neuropharmacology *83*, 1–8.

Maurano, M.T., Humbert, R., Rynes, E., Thurman, R.E., Haugen, E., Wang, H., Reynolds, A.P., Sandstrom, R., Qu, H., Brody, J., et al. (2012). Systematic localization of common disease-associated variation in regulatory DNA. Science *337*, 1190–1195.

Maze, I., Covington, H.E., 3rd, Dietz, D.M., LaPlant, Q., Renthal, W., Russo, S.J., Mechanic, M., Mouzon, E., Neve, R.L., Haggarty, S.J., et al. (2010). Essential role of the histone methyltransferase G9a in cocaine-induced plasticity. Science *327*, 213–216.

McIntyre, J.C., Titlow, W.B., and McClintock, T.S. (2010). Axon growth and guidance genes identify nascent, immature, and mature olfactory sensory neurons. J. Neurosci. Res. *88*, 3243–3256.

Mitsui, S., Yamaguchi, S., Matsuo, T., Ishida, Y., and Okamura, H. (2001). Antagonistic role of E4BP4 and PAR proteins in the circadian oscillatory mechanism. Genes Dev. *15*, 995–1006.

Nau, F., Jr., Miller, J., Saravia, J., Ahlert, T., Yu, B., Happel, K.I., Cormier, S.A., and Nichols, C.D. (2015). Serotonin 5-HT_2 receptor activation prevents allergic asthma in a mouse model. Am. J. Physiol. Lung Cell. Mol. Physiol. *308*, L191–L198.

Nichols, D.E. (2016). Psychedelics. Pharmacol. Rev. *68*, 264–355.

Nichols, C.D., and Sanders-Bush, E. (2002). A single dose of lysergic acid diethylamide influences gene expression patterns within the mammalian brain. Neuropsychopharmacology *26*, 634–642.

Nord, A.S., and West, A.E. (2020). Neurobiological functions of transcriptional enhancers. Nat. Neurosci. *23*, 5–14.

Olson, D.E. (2020). The Subjective Effects of Psychedelics May Not Be Necessary for Their Enduring Therapeutic Effects. ACS Pharmacol. Transl. Sci. *4*, 563–567.

Pais, A.B., Pais, A.C., Elmisurati, G., Park, S.H., Miles, M.F., and Wolstenholme, J.T. (2019). A Novel Neighbor Housing Environment Enhances Social Interaction and Rescues Cognitive Deficits from Social Isolation in Adolescence. Brain Sci. *9*, 336.

Peñagarikano, O., and Geschwind, D.H. (2012). What does CNTNAP2 reveal about autism spectrum disorder? Trends Mol. Med. *18*, 156–163.

Picelli, S., Björklund, A.K., Faridani, O.R., Sagasser, S., Winberg, G., and Sandberg, R. (2013). Smart-seq2 for sensitive full-length transcriptome profiling in single cells. Nat. Methods *10*, 1096–1098.

Picelli, S., Faridani, O.R., Björklund, A.K., Winberg, G., Sagasser, S., and Sandberg, R. (2014). Full-length RNA-seq from single cells using Smart-seq2. Nat. Protoc. *9*, 171–181.

Quinlan, A.R., and Hall, I.M. (2010). BEDTools: a flexible suite of utilities for comparing genomic features. Bioinformatics *26*, 841–842.

Ray, T.S. (2010). Psychedelics and the human receptorome. PLoS ONE *5*, e9019, e9019.

Rodenas-Cuadrado, P., Pietrafusa, N., Francavilla, T., La Neve, A., Striano, P., and Vernes, S.C. (2016). Characterisation of CASPR2 deficiency disorder–a syndrome involving autism, epilepsy and language impairment. BMC Med. Genet. *17*, 8.

Ross-Innes, C.S., Stark, R., Teschendorff, A.E., Holmes, K.A., Ali, H.R., Dunning, M.J., Brown, G.D., Gojis, O., Ellis, I.O., Green, A.R., et al. (2012). Differential oestrogen receptor binding is associated with clinical outcome in breast cancer. Nature *481*, 389–393.

Rousseeuw, P.J. (1987). Silhouettes: A graphical aid to the interpretation and validation of cluster analysis. J. Comput. Appl. Math. *20*, 53–65.

Sánchez-González, A., Thougaard, E., Tapias-Espinosa, C., Cañete, T., Sampedro-Viana, D., Saunders, J.M., Toneatti, R., Tobeña, A., Gónzalez-Maeso, J., Aznar, S., and Fernández-Teruel, A. (2021). Increased thin-spine density in frontal cortex pyramidal neurons in a genetic rat model of schizophrenia-relevant features. Eur. Neuropsychopharmacol. *44*, 79–91.

Savalia, N.K., Shao, L.X., and Kwan, A.C. (2021). A Dendrite-Focused Framework for Understanding the Actions of Ketamine and Psychedelics. Trends Neurosci. *44*, 260–275..

Schmid, Y., Enzler, F., Gasser, P., Grouzmann, E., Preller, K.H., Vollenweider, F.X., Brenneisen, R., Müller, F., Borgwardt, S., and Liechti, M.E. (2015). Acute

Effects of Lysergic Acid Diethylamide in Healthy Subjects. Biol. Psychiatry *78*, 544–553.

Shannon, P., Markiel, A., Ozier, O., Baliga, N.S., Wang, J.T., Ramage, D., Amin, N., Schwikowski, B., and Ideker, T. (2003). Cytoscape: a software environment for integrated models of biomolecular interaction networks. Genome Res. *13*, 2498–2504.

Shao, L.X., Liao, C., Gregg, I., Davoudian, P.A., Savalia, N.K., Delagarza, K., and Kwan, A.C. (2021). Psilocybin induces rapid and persistent growth of dendritic spines in frontal cortex in vivo. Neuron *109*, 2535–2544.e4.

Spruston, N. (2008). Pyramidal neurons: dendritic structure and synaptic integration. Nat. Rev. Neurosci. *9*, 206–221.

Tovote, P., Fadok, J.P., and Lüthi, A. (2015). Neuronal circuits for fear and anxiety. Nat. Rev. Neurosci. *16*, 317–331.

Ventéo, S., Desiderio, S., Cabochette, P., Deslys, A., Carroll, P., and Pattyn, A. (2019). Neurog2 Deficiency Uncovers a Critical Period of Cell Fate Plasticity and Vulnerability among Neural-Crest-Derived Somatosensory Progenitors. Cell Rep. *29*, 2953–2960.

Vollenweider, F.X., Vollenweider-Scherpenhuyzen, M.F., Bäbler, A., Vogel, H., and Hell, D. (1998). Psilocybin induces schizophrenia-like psychosis in humans via a serotonin-2 agonist action. Neuroreport *9*, 3897–3902.

Wang, L., Wang, Y., Duan, C., and Yang, Q. (2018). Inositol phosphatase INPP4A inhibits the apoptosis of *in vitro* neurons with characteristic of intractable epilepsy by reducing intracellular Ca^{2+} concentration. Int. J. Clin. Exp. Pathol. *11*, 1999–2007.

Yaden, D.B., and Griffiths, R.R. (2020). The Subjective Effects of Psychedelics Are Necessary for Their Enduring Therapeutic Effects. ACS Pharmacol. Transl. Sci. *4*, 568–572.

Yu, G., Wang, L.G., Han, Y., and He, Q.Y. (2012). clusterProfiler: an R package for comparing biological themes among gene clusters. OMICS *16*, 284–287.

Yu, G., Wang, L.G., and He, Q.Y. (2015). ChIPseeker: an R/Bioconductor package for ChIP peak annotation, comparison and visualization. Bioinformatics *31*, 2382–2383.

Zagnoni, P.G., and Albano, C. (2002). Psychostimulants and epilepsy. Epilepsia *43* (*Suppl 2*), 28–31.

Zanos, P., Highland, J.N., Stewart, B.W., Georgiou, P., Jenne, C.E., Lovett, J., Morris, P.J., Thomas, C.J., Moaddel, R., Zarate, C.A., Jr., and Gould, T.D. (2019). (*2R,6R*)-hydroxynorketamine exerts $mGlu_2$ receptor-dependent antidepressant actions. Proc. Natl. Acad. Sci. USA *116*, 6441–6450.

Zhang, B., and Horvath, S. (2005). A general framework for weighted gene coexpression network analysis. Stat. Appl. Genet. Mol. Biol. *4*, Article17.

Zhang, Y., Liu, T., Meyer, C.A., Eeckhoute, J., Johnson, D.S., Bernstein, B.E., Nusbaum, C., Myers, R.M., Brown, M., Li, W., and Liu, X.S. (2008). Model-based analysis of ChIP-Seq (MACS). Genome Biol. *9*, R137.

Zhang, G., Ásgeirsdóttir, H.N., Cohen, S.J., Munchow, A.H., Barrera, M.P., and Stackman, R.W., Jr. (2013). Stimulation of serotonin 2A receptors facilitates consolidation and extinction of fear memory in C57BL/6J mice. Neuropharmacology *64*, 403–413.

Zhu, B., Hsieh, Y.P., Murphy, T.W., Zhang, Q., Naler, L.B., and Lu, C. (2019). MOWChIP-seq for low-input and multiplexed profiling of genome-wide histone modifications. Nat. Protoc. *14*, 3366–3394.

Zonta, B., Tait, S., Melrose, S., Anderson, H., Harroch, S., Higginson, J., Sherman, D.L., and Brophy, P.J. (2008). Glial and neuronal isoforms of Neurofascin have distinct roles in the assembly of nodes of Ranvier in the central nervous system. J. Cell Biol. *181*, 1169–1177.

STAR★METHODS

KEY RESOURCES TABLE

REAGENT or RESOURCE	SOURCE	IDENTIFIER
Antibodies		
Alexa 488 conjugated anti-NeuN	Millipore	Cat# MAB377X; RRID: AB_2149209
anti-H3K27ac	Active Motif	Cat# 39135; RRID: AB_2614979
Bacterial and virus strains		
AAV8.CamKIIα.eYFP	UNC Vector Core	Custom order
Chemicals, peptides, and recombinant proteins		
(±) DOI (1-(2,5-dimethoxy-4-iodophenyl)-2-aminopropane hydrochloride)	Sigma Aldrich	Cat# D101
Isoflurane	Henry Schein	Cat# 1182097
Protease Inhibitor Cocktail	Sigma Aldrich	Cat# P8340-5ML
Recombinant Ribonuclease Inhibitor	Takara Bio	Cat# 2313B
OptiPrep Density Gradient Medium	Sigma Aldrich	Cat# D1556-250ML
Normal Goat Serum (10%)	Life Technologies	Cat# 50062Z
Micrococcal Nuclease	Thermo Scientific	Cat# PI88216
SPRIselect beads	Beckman Coulter	Cat# B23317
Superscript II reverse transcriptase	Life Technologies	Cat# 18064014
KAPA HiFi HotStart ReadyMix	KAPA Biosystems	Cat# KK2601
dNTP mix	Life Technologies	Cat# 18427088
Critical commercial assays		
Locomotor activity monitoring	Omnitech Inc	Fusion V5.3
Pre-pulse inhibition of the startle	San Diego Instruments	SR-LAB Startle Response System
Fear acquisition and extinction	Med Associates	MED-VFCNIR-M
Confocal microscopy	Carl Zeiss	CLM710
Voltage-clamp recording	Molecular Devices	Multiclamp 700B amplifier, Digitizer 1140A, Cornerstone S-900 stimulator
Cell Sorter	BD Biosciences	BD FACSAria III
RNAeasy mini kit	QIAGEN	Cat #74104
RNase-Free DNase Set	QIAGEN	Cat #79254
Nextera XT DNA Library Prep kit	Illumina	Cat# FC-131-1024
ACCEL-NGS 2S Plus DNA library kit	Swift Biosciences	Cat# 21024
2S Indexing Kit	Swift Biosciences	Cat# 26396
Sequencing platform	Illumina	Illumina Hi-seq 4000
High Sensitivity DNA analysis kit	Agilent	Cat# 5067-4626
TapeStation	Agilent	Ca# 2200
KAPA library quantification	Kapa Bio	Cat# KK4809
Deposited data		
ChIP-seq and RNA-seq raw and processed data	Gene Expression Omnibus	GEO: GSE161626
Experimental models: Organisms/strains		
Mouse 129S6/SvEv	Taconic Farms	Cat #129SVE-M
Mouse C57BL/6NTac	Taconic Farms	Cat # B6-M
Mouse *5-HT$_{2A}$R$^{-/-}$*	González-Maeso et al., 2007	N/A
Mouse C57BL/6J	JAXS	Cat #00064

(*Continued on next page*)

Continued		
REAGENT or RESOURCE	SOURCE	IDENTIFIER
Oligonucleotides		
TSO: AAGCAGTGGTATCAACGCAGAG TACATrGrG+G (rG: riboguanosines; +G: LNA-modified guanosine)	Integrated DNA Technologies	N/A
Oligo-dT30VN: AAGCAGTGGTATCAACG CAGAGTACT30VN (N: any base; V: T, C or G)	Integrated DNA Technologies	N/A
ISPCR oligo: AAGCAGTGGTATCAACGCAGAGT	Integrated DNA Technologies	N/A
Software and algorithms		
NeuronStudio	Mount Sinai Imaging Center	v0.9.92 https://biii.eu/neuronstudio
Prism	GraphPad	v9 https://www.graphpad.com/scientific-software/prism/
Voltage-clamp recording	Molecular Devices	clampex 10.2 https://support.moleculardevices.com/
Voltage-clamp offline analysis	Molecular Devices	Campfit 10.2 https://support.moleculardevices.com/s/
Trim Galore!	N/A	https://github.com/FelixKrueger/TrimGalore
Bowtie2	(Langmead and Salzberg, 2012)	https://github.com/BenLangmead/bowtie2
MACS2	Zhang et al., 2008	https://github.com/macs3-project/MACS
SAMTools	Li et al., 2009	https://github.com/samtools/samtools
BEDTools	(Quinlan and Hall, 2010)	https://github.com/arq5x/bedtools
SeqMonk	N/A	https://www.bioinformatics.babraham.ac.uk/projects/seqmonk/ RRID: SCR_001913
HISAT2	Kim et al., 2015	http://daehwankimlab.github.io/hisat2/
FeatureCounts	(Liao et al., 2014)	http://subread.sourceforge.net/
DESeq2	Love et al., 2014	https://bioconductor.org/packages/release/bioc/html/DESeq2.html
WGCNA	(Langfelder and Horvath, 2008)	https://cran.r-project.org/web/packages/WGCNA/index.html
Other		
KIMBLE Dounce tissue grinder set	Sigma aldrich	Cat# D9063

RESOURCE AVAILABILITY

Lead contact

Further information and requests for resources and reagents should be directed to and will be fulfilled by the Lead Contact, Javier González-Maeso (javier.maeso@vcuhealth.org).

Materials availability

This study did not generate new unique reagents

Data and code availability

- ChIP-seq and RNA-seq datasets are deposited in the Gene Expression Omnibus (GEO) repository with the following accession number: GEO: GSE161626.
- This paper does not report original code.
- Any additional information required to reanalyze the data reported in this paper is available from the lead contact upon request.

EXPERIMENTAL MODEL AND SUBJECT DETAILS

Experiments were performed on adult (10 – 20 weeks old) male mice randomly allocated into the different pre-treatment groups. Animals were housed on a 12 h light/dark cycle at 23°C with food and water *ad libitum*, except during behavioral testing (always

during the light cycle). All procedures were conducted in accordance with NIH guidelines and were approved by the Virginia Commonwealth University Animal Care and Use Committee. All efforts were made to minimize animal suffering and the number of animals used. Drug/s were administered (i.p.) diluted in saline (0.9%); vehicle refers to the saline solution alone. Experiments involving dendritic spine structure, synaptic plasticity, and ChIP-seq/RNA-seq techniques were conducted in 129S6/SvEv mice (Taconic). Experiments involving functional synaptic plasticity (LTP) behavior assays that required only the inclusion of wild-type animals were conducted in C57BL/6 mice (Taconic). For fear acquisition and extinction assays, experiments were conducted in *5-HT$_{2A}$R$^{+/+}$* and *5-HT$_{2A}$R$^{-/-}$* mice that were offspring of heterozygote breeding(González-Maeso et al., 2007). Breeders were backcrossed from 129S6/SvEv onto C57BL/6 (JAXS) for several generations (F5 was used for behavioral paradigms).

METHOD DETAILS

Locomotor activity

Locomotor activity was monitored as previously described (Hideshima et al., 2018), with minor changes. Briefly, animals were injected with DOI (2 mg/kg, i.p.) or vehicle and immediately returned to their home cage. Evaluation of locomotor activity was conducted 24h after drug administration on a computerized three-dimensional activity monitoring system (Fusion v5.3; Omnitech Electronics Inc.) that interpolates the animal's activity from interruption of infrared beams traversing the different planes of space. Mice were allowed to acclimate to the behavioral room for 1h prior to monitoring their individual locomotor activity on a commercial Plexiglas open field (25 × 25 × 20 cm) for 90 min. Horizontal activity is measured as the collapsed amount of beam interruptions in the *x-y* planes in 5 min periods. The open field was cleaned with 1% Roccal-D in between sessions.

Light-dark boxes preference

Animals were injected with DOI (2 mg/kg, i.p.) or vehicle and immediately returned to their home cage. Preference for light or dark environment as a proxy for anxiety-like behaviors was assessed 18h after drug administration using a commercial open field in which space is equally divided into light and dark areas (25 × 12 × 20 cm each) connected through a small (5 × 5 cm) opening (Pais et al., 2019). The tracking system (Fusion v5.3; Omnitech Electronics Inc.) infers animal activity and position from interruptions to infrared beams traversing the different planes of space. After 1h acclimation to the behavioral room, mice were individually placed in the entrance to the dark compartment. The study monitored their preference for each area (light/dark) expressed as the percentage of time spent on each. The chambers were cleaned with 1% Roccal-D in between sessions. After completion of the experiment mice were returned to their home-cages.

Forced-swimming test

The procedure was conducted 24h after DOI (2 mg/kg, i.p.) or vehicle administration (including a 1h acclimation to the behavioral room). 2 L (12.5 cm diameter × 21 cm height) beakers were 2/3-filled with water (~23°C). Mice were carefully introduced in the containers while being held by the tail so that the head would remain over the water line during the animal immersion. Sessions were recorded on digital video camera and immobility was scored during the last 4 min of the 6 min session by a trained analyst blind to the pre-treatment. Immobility was defined as passive floating with no additional activity except that needed to maintain the head of the animal above the water level (Zanos et al., 2019).

Novel object recognition

Assays were conducted as previously reported (Ibi et al., 2017; de la Fuente Revenga et al., 2018), with minor modifications. Briefly, the testing arena consisted of an opaque rectangular plastic container with open top (32 × 20 × 23 cm). The objects employed (tissue culture flasks filled with wood chips and opaque white light bulbs) were of comparable volume and height (~10 cm) and were attached to the bottom of the container with double-side tape 10 cm away from the walls. Both the objects and chambers were cleaned thoroughly with diluted ethanol between tests to remove olfactory cues. Preference for a novel object — as opposed to a familiar one — was tested on mice that received DOI (2 mg/kg, i.p.) or vehicle 24h prior. Mice were allowed to get acclimate to the behavioral room for the duration of the whole session (at least 1h prior to the test). The test consisted of three stages, a 20 min habituation to the field, a 5 min acquisition trial in which two identical objects were present in the field and a 5 min recognition trial in which one of the identical objects had been replaced by a novel one. All stages were separated by 5 min during which the animals were returned to their home cage. Object exploration was defined as the animal licking, sniffing or touching the object with the forepaws while sniffing. Climbing an object was not considered in the exploration time. The exploration time for each side (same object on both sides) during the acquisition and the exploration time for the novel object during the recognition was assessed on digital video camera recordings by a trained analyst blind to the pre-treatment. The exploratory preference for the novel object was calculated as percentage of total exploratory time spent exploring the novel object during the recognition stage. Place preference was controlled during the acquisition stage and by alternating the position of the novel object between left and right during the recognition stage.

Prepulse inhibition of startle

Assays were conducted as previously reported (Kurita et al., 2012) with minor modifications. Briefly, recording of the startle magnitude in response to acoustic stimuli was performed using the SR-LAB Startle Response System (San Diego Instruments). Mice

that had received DOI (2 mg/kg) or vehicle 24h prior were presented with a startling stimulus of 119 dB (20 ms) preceded (80 ms interstimulus interval), or not, by (20 ms) prepulses of 73 dB, 77 dB and 85 dB (20 ms). Background noise was set to 69 dB. Mice were habituated to the testing room at least 1h prior to the start of the experiment. The experiment proceeded as follows: Animals were placed in the mouse-sized startle chambers and allowed to acclimate to chamber and background noise for 5 min. Mice were presented with 5 stimulus-only trials at the beginning and the end of the session (used for control, but not included in the analysis). During the session, animals were randomly subjected to 65 trials in five different categories (13 of each): stimulus-only, no stimulus, 73 dB prepulse and stimulus, 77 dB prepulse and stimulus, 85 dB prepulse and stimulus. Each session lasted about a total of 30 min. Prepulse inhibition of startle (PPI) for each prepulse and trial was determined as percentage of the startle amplitude (V_{max}) of the prepulse+stimulus trial relative to the average of the startle amplitude (V_{max}) for the 13 stimulus-only trials.

Contextual fear acquisition and extinction

Fear conditioning tests were conducted using two commercially supplied Near Infrared Video Freeze Systems controlling each testing chamber (MED-VFCNIR-M, Med Associates, Inc., St. Albans, VT), each operating four test chambers. Each polycarbonate test chamber (32 × 25 × 25 cm) was equipped with a metal grid floor and was enclosed in a sound-attenuated box (63.5 × 35.5 × 76 cm). Video images at 30 fps (640 × 480 pixels, down-sampled to ~1 pixel per visible mm^2) were collected. A freezing event was automatically designated if the absence of movement was 1 s or longer (*i.e.*, negligible variation in the pixel composition in between frames for 30 consecutive frames). Mice were acclimated to the behavioral testing room (with white noise in the background) for at least 1h in the 2 days prior to experimental sessions. White noise was present at all times when the animals were held in the testing room. Mice were handled for 2 min (each) on the 2 days prior to the start of the testing. Two different contexts (A and B) with different spatial, visual and olfactory cues were employed. Context A was composed of a standard polycarbonate squared cage (see dimensions above) with metallic walls and shock-delivering grid on the floor, with visible and IR illumination, and with lemon scent (artificial lemon flood flavoring) on the bedding. Context B was a modified chamber with a black triangular adaptor, white opaque plastic continuous floor, without visible light but with IR light and cardamom scent (cardamom artificial food flavoring) on the bedding. Experimental sessions were performed on two consecutive days. On day 1, fear-acquisition was established in Context A. The acquisition stage period conditioned the mice to associate the context (A) with a noxious stimulus (foot-shocks). After a 90 s stimulus-free period at the beginning of the experiment (baseline), mice received 6 unconditioned stimuli consisting of 2 s scrambled 0.70 mA foot-shocks delivered through the grid floor separated by 90 s inter-stimulus intervals. Freezing time was measured as described above during the baseline and during the inter-stimulus intervals. For all other periods, freezing time was measured in 5 min units. Animals were returned to their home cages immediately after completion of the 90 s period following the last foot-shock. After a 2h holding period, the expression stage followed. Animals were placed in Context A for 5 min. During this time, foot-shocks were not delivered. This period served as a control for conditioning and preliminary extinction training (noxious stimulus-free Context A). Depending on testing conditions, DOI (2 mg/kg, i.p.) or vehicle was administered 10 min after the expression stage or 24h prior to the acquisition stage. At the end of the experimental session animals were returned to the vivarium. On day 2, the generalization of the fear response was evaluated in Context B for 5 min. The purpose of this test was to evaluate and quantify the expression of generalization of fear in a novel context (*i.e.*, expression of freezing behavior in a novel environment). Mice were held for 2 additional hours in their home cage prior to the extinction test. During extinction training, mice were returned to Context A for 20 min and observed for freezing behavior over time in periods of 5 min in the absence of any aversive stimuli.

Dendritic spine analysis

Dendritic spine analysis assays were carried out as previously reported (Ibi et al., 2017), with minor modifications. Briefly, adeno-associated virus (AAV) serotype 8 expressing eYFP under the *CaMKIIα* promoter was produced at the University of North Carolina at Chapel Hill Vector Core. Mice were anesthetized with isoflurane during the surgery and perfusion. The virus was delivered bilaterally with a Hamilton syringe at a rate of 0.1 μl/min for a total volume of 0.5 μl on each side. The following coordinates were used: +1.6 mm rostrocaudal, −2.4 mm dorsoventral, and +2.6 mm mediolateral from bregma (relative to dura) with a 10°C lateral angle. Previous findings have validated expression of eYFP in CaMKIIα-positive neurons, but not in parvalbumin-positive neurons in the frontal cortex (Ibi et al., 2017). All experiments were performed at least three weeks after surgery, when transgene expression is maximal (Ibi et al., 2017). For spine analysis, apical dendritic segments 50-150 μm away from the soma were randomly chosen from AAV-infected cells that express eYFP. Images were acquired from a 4% paraformaldehyde-fixed 50 μm coronal slice, using a confocal fluorescence microscope (CLSM710, Carl Zeiss). CaMKIIα-positive pyramidal neurons in L5 expressing eYFP were confirmed by their characteristic triangular somal shape. To qualify for spine analysis, dendritic segments had to satisfy the following requirements: (i) the segment had to be completely filled (all endings were excluded), (ii) the segment must have been at least 50 μm from the soma, and (iii) the segment could not be overlapping with other dendritic branches. Dendritic segments were imaged using a × 63 lens (numerical aperture 1.46; Carl Zeiss) and a zoom of 2.5. Pixel size was 0.09 μm in the x-y plane and 0.2 μm in the z plane. Images were taken with a resolution of 1024 × 300 (the y dimension was adjusted to the particular dendritic segment to expedite imaging), the pixel dwell time was 1.27 μm/s and the line average was set to 4. Only one dendrite per neuron on 4-5 neurons per animal per experimental group was analyzed. For quantitative analysis of spine size and shape, NeuronStudio was used with the rayburst algorithm described previously (Ibi et al., 2017). NeuronStudio classifies spines as stubby, thin or mushroom on the basis of the following values: (i) aspect ratio, (ii) head-to-neck ratio and (iii) head diameter. Spines with a neck can be classified as either thin or

mushroom, and those without a neck are classified as stubby. Spines with a neck are labeled as thin or mushroom on the basis of head diameter. These parameters have been verified by comparison with trained human operators fully blinded across groups.

Whole-cell patch-clamp recordings and LTP induction

Whole-cell patch clamp recordings from neurons in layers 2/3 (L2/3) of somatosensory cortex were obtained from 8-10-week-old male mice as previously described (Ibi et al., 2017). Prior to recording, mice were housed in pairs, with one mouse of each pair designated an "experimental" mouse and the other mouse designated a "companion." Twenty-four hours prior to recording, experimental mice of each pair received a single injection (i.p.) of either saline (controls, n = 5) or DOI (2,5-Dimethoxy-4-iodoamphetamine hydrochloride; 2 mg/kg, n = 5). The investigator performing the recordings was blind to treatment condition. Companion mice, who received a single saline injection at the same time as experimental mice, were used to match housing/social conditions across control and DOI experimental animals in the 24 hr period prior to recording, but were then discarded. Experimental mice were deeply anesthetized with isoflurane and decapitated. Brains were rapidly removed and submerged in chilled (~4°C) sucrose-artificial cerebrospinal fluid (sucrose-aCSF; 233.7 mM sucrose, 26 mM $NaHCO_3$, 3 mM KCl, 8 mM $MgCl_2$, 0.5 mM $CaCl_2$, 20 mM glucose and 0.4 mM ascorbic acid) that was continuously bubbled with carbogen (95% O_2–5% CO_2). Acute coronal slices (350 μm-thick) were sectioned on a VT1000S vibratome (Leica) and transferred to a recovery chamber bubbled with carbogen and aCSF (117 mM NaCl, 4.7 mM KCl, 1.2 mM $MgSO_4$, 2.5 mM $CaCl_2$, 1.2 mM NaH_2PO_4, 24.9 mM $NaHCO_3$ and 11.5 mM glucose) for 1h at room temperature. Slices were transferred to the recording chamber and perfused with 31°C oxygenated aCSF containing the $GABA_A$ receptor antagonist gabazine (10 μM). Whole-cell electrodes were pulled from borosilicate glass (pipette resistance 3–4 MΩ) and filled with (in mM): 120 Cs-methanesulfonate, 10 HEPES, 0.5 EGTA, 8 NaCl, 5 TEA-CL, 4 Mg-ATP, 0.4 NaGTP, and 10 phosphocreatine. Internal solution was adjusted to 280–290 mOsm and 7.3 pH. L2/3 neurons chosen for recording had pyramidal-shaped somata. Following formation of a gigaseal, the neuronal membrane was ruptured and set to a holding potential of −70 mV and allowed to equilibrate for ~3 mins. Subsequent recordings were carried out in voltage-clamp mode with a Multiclamp 700B amplifier (Molecular Devices). Analog signals were low-pass filtered at 2 kHz, digitized at 5 kHz and analyzed with pClamp 10 software (Molecular Devices). LTP of L4 to L2/3 synapses was elicited using a pairing-protocol in which presynaptic stimulation of L4 was paired with brief postsynaptic depolarization of L2/3 neurons situated within the same column as described previously (Ibi et al., 2017). A tungsten concentric bipolar electrode was placed in L4 and used to evoke excitatory postsynaptic currents (EPSCs) in overlying L2/3 neurons at 0.1 Hz through the entire experiment. EPSCs evoked by L4 stimulation were recorded at −70 mV for a baseline period of ~3-5 mins, followed by brief membrane depolarization to 0 mV for 10 mins, then the holding potential was returned to −70mV for the duration of 35-40 mins. Series resistance was measured at the beginning and end of each recording. Any neuron showing > 30% change was discarded from the experiment. Offline analysis was conducted with Clampfit software (Molecular Devices). Mean EPSC amplitudes were normalized to their respective averaged baseline values. Data are plotted as percent change from averaged baseline values.

Nuclei isolation and sorting via FACS

Nuclei isolation was conducted using a published protocol (Lake et al., 2016; Zhu et al., 2019). All steps were conducted on ice, and all centrifugation was conducted at 4°C. One piece of mouse frontal cortex tissue (6-10 mg) was placed in 3 mL of ice-cold nuclei extraction buffer (NEB) [0.32 M sucrose, 5 mM $CaCl_2$, 3 mM $Mg(Ac)_2$, 0.1 mM EDTA, 10 mM tris-HCl, and 0.1%(v/v) Trition X-100] with 30 μL of freshly added protease inhibitor cocktail (PIC, Sigma-Aldrich), 3 μL of 100 mM phenylmethylsulfonyl fluoride (PMSF, Sigma-Aldrich) in Isopropyl alcohol, 3 μL of 1 M dithiothreitol (DTT, Sigma-Aldrich), and 4.5 μL of ribonuclease (RNase) inhibitor (2313A,Takara Bio). The tissue was homogenized in a tissue grinder (D9063, Sigma-Aldrich). The homogenate was filtered with a 40 μm cell strainer (22-363-547, Thermo Fisher Scientific) and collected in a 15 mL centrifuge tube. The cell suspension was centrifuged at 1000 RCF for 10 min. The supernatant was discarded, and the pellet was resuspended in 0.5 mL of ice-cold NEB with 5 μL of freshly added PIC, 0.5 μL of PMSF, 0.5 μL of DTT, and 0.75 μL of RNase inhibitor. 500 μL of the sample was mixed with 750 μL of 50%(w/v) iodixanol (made by mixing 4 mL of OptiPrep™ gradient (Sigma-Aldrich) and 0.8 mL of diluent [150 mM KCl, 30 mM $MgCl_2$, and 120 mM tris-HCl]). The mixture was centrifuged at 10,000 RCF for 20 min. Then, the supernatant was removed and 300 μL of 2%(w/v) normal goat serum (50062Z, Life technologies) in Dulbecco's PBS (DPBS, Life technologies) was added to resuspend the nuclei pellet. To separate $NeuN^+$ and $NeuN^-$ fractions, 6 μL of 2 ng/μl anti-NeuN antibody conjugated with Alexa 488 (MAB377X, Millipore) in DPBS was added into the nuclei suspension. The suspension was mixed well and incubated at 4°C for 1 h on a rotator mixer (Labnet). After incubation, the sample was sorted into $NeuN^+$ and $NeuN^-$ fractions using a BD FACSAria™ cell sorter (BD Biosciences). The sorted $NeuN^+$ nuclei were directly used for RNA-seq experiment. 200 μL of sorted $NeuN^+$ nuclei suspension, containing ~26,000 nuclei, was added into 800 μL of ice-cold PBS for ChIP-seq experiment. 200 μL of 1.8 M sucrose solution, 10 μL of 1 M $CaCl_2$, and 3 μL of 1 M $Mg(Ac)_2$ were added into the mixture. The solution was mixed well and incubated on ice for 15 min. Then, the sample was centrifuged at 1800 RCF at 4°C for 15 min. The supernatant was discarded and the pellet was resuspended in 60 μL of PBS with 0.6 μL of freshly added PIC and 0.6 μL of PMSF and stored on ice until use for ChIP-seq.

Construction of ChIP-seq libraries

~10,000 $NeuN^+$ nuclei were used to produce each ChIP-seq library and two technical replicates were generated for each brain sample. 6 brain samples were processed under each treatment condition. One input per sample was generated using ~4,000 nuclei. ChIP

was carried out using multiplexed MOWChIP-seq with MNase digestion for chromatin fragmentation and anti-H3K27ac (39135, Active Motif) antibody, following a published protocol (Zhu et al., 2019).

Construction of RNA-seq libraries

~5000 NeuN$^+$ nuclei were used to produce each RNA-seq library and two technical replicates were generated for each brain sample. 6 brain samples were processed under each treatment condition. RNA extraction from 50 μL of nuclei suspension from FACS (containing 5000 sorted NeuN$^+$ nuclei) was conducted using RNeasy Mini Kit (74104, QIAGEN) and RNase-Free DNase Set (79254, QIAGEN), following the manufacturer's instruction. Extracted mRNA in 30-μl volume was concentrated by ethanol precipitation and resuspended in 4.6 μL of RNase-free water. cDNA was prepared using the SMART-seq2 protocol (Picelli et al., 2013) with minor modification. ~2 ng of mRNA in 4.6 μl of water was mixed with 2 μL of 100 μM oligo-dT primer and 2 μL of 10 mM dNTP mix. After being denatured at 72°C for 3 min, the mRNA solution was immediately placed on ice. 11.4 μL of reverse transcript mix [made from 1 μL of SuperScript II reverse transcriptase (200 U/μl), 0.5 μL of RNase inhibitor (40 U/μl), 4 μL of Superscript II first-strand buffer, 1 μL of DTT (100mM), 4 μL of 5 M Betaine, 0.12 μL of 1 M $MgCl_2$, 0.2 μL of TSO (100 μM), 0.58 μL of nuclease-free water] was mixed with the mRNA solution and the mixture was incubated at 42°C for 90 min, followed by 10 cycles of (50°C for 2 min, 42°C for 2 min). The reaction was finally inactivated at 70°C for 15 min. 20 μL of first-strand mixture was then mixed with 25 μL of KAPA HiFi HotStart ReadyMix, 0.5 μL of (100 μM) IS PCR primers, 0.5 μL of Evagreen dye, and 4 μL of nuclease-free water. Generated cDNA was amplified by incubation at 98°C for 1 min, followed by 9-11 cycles of (98°C 15 s, 67°C 30 s, 72°C 6 min). After PCR amplification, 50 μL of PCR mix was purified by using 50 μL of SPRIselect beads. ~600 pg of purified cDNA was used to produce a RNA-seq library using Nextera XT DNA Library Preparation kit (FC-131-1024, Illumina), following the manufacturer instructions.

Sequencing

The fragment size of ChIP-seq and RNA-seq libraries was measured using high sensitivity DNA analysis kit (5067-4626, Agilent) on a TapeStation system (2200, Agilent). The concentration of each library was examined using a KAPA library quantification kit (KK4809, Kapa Biosystems), and then the quantified libraries were pooled at 10 nM. The libraries were sequenced by Illumina HiSeq 4000 with single-end 50-nt read. Around 15 million reads were generated for each ChIP-seq library, 10 million reads for each input library, and 11 million reads for each RNA-seq library.

ChIP-seq reads alignment and normalization

Sequencing reads were trimmed using default settings by Trim Galore! (Babraham Institute, https://www.bioinformatics.babraham.ac.uk/projects/trim_galore/). Trimmed reads were aligned to the mm10 genome with Bowtie2 (Langmead and Salzberg, 2012). Peaks were called using MACS2 (Zhang et al., 2008) ($q < 0.05$). Blacklisted regions in the mm10 as defined by ENCODE were removed to improve data quality using SAMtools (Li et al., 2009). Mapped reads from ChIP and input samples were extended by 100 bp on either side (250 bp total) using BEDtools and a normalized signal was calculated (Quinlan and Hall, 2010).

$$Normalized\ Signal = \left(\frac{ChIP\ Signal}{No.\ of\ ChIP\ Reads} - \frac{Input\ Signal}{No.\ of\ Input\ Reads}\right) \times 10^6$$

For visualization in IGV (Broad Institute), the signal was calculated in 100bp windows over the entire genome and output as a bigWig file.

Differential enhancers

We first predicted enhancer regions (1000 bp in width with peak summit ± 500 bp) by identifying H3K27ac peaks that did not intersect with promoters (defined as TSS ± 2000 bp) (Cao et al., 2015). Consensus enhancer sets were generated for each experimental group (VEH, 24 h, 48 h and 7d) using Diffbind (Ross-Innes et al., 2012) and then combined to generate an overall consensus enhancer set. In the process, a majority rule was applied to identify the consensus enhancers when all technical/biological replicates were considered. For example, among all 12 replicates of H3K27ac datasets in one experimental group, a consensus enhancer must be present in at least 7. Differential enhancers between any two experimental groups were identified from the overall consensus enhancer set using the bioconductor DESeq2 package (Love et al., 2014) (FDR < 0.05) with Benjamini-Hochberg method (Benjamini and Hochberg, 1995).

K-means clustering, GO term analysis, TF motif analysis

We also performed K-means clustering on differential enhancers and DEGs across experimental groups. In each row, the values (x) were normalized by dividing by $\sqrt{sum(x^2)}$. The optimal number of clusters was determined using Silhouette method (Rousseeuw, 1987). We created a list of the enhancer target genes by examining the correlation between gene expression (as reflected by RNA-seq data) and H3K27ac intensity at the candidate enhancers (Gorkin et al., 2020). Compared to assigning an enhancer to its nearest gene, this approach produces a much higher percentage of enhancer-gene pairs that match the results determined experimentally using techniques including Hi-C (Gorkin et al., 2020). All the enhancers that were not linked with their target genes after the step were then processed using ChIPSeeker (Yu et al., 2015) with default condition and TxDb.Mmusculus.UCSC.mm10.knownGene

to link to their nearest genes (as target genes). All the target genes identified, either by correlation between H3K27ac and RNA-seq or by linking with nearest genes, were combined for downstream analysis. GO biological processes enrichment test was performed using the bioconductor clusterProfiler (Yu et al., 2012) package (with FDR adjusted p value < 0.01). Motif analysis was also performed to determine enriched transcription factor binding motifs among the enhancer regions using Homer (Heinz et al., 2010) (with options –size 200 –p 16, and q-value < 0.01).

GWAS loci association

Peak locations were converted from mm10 to hg19 through UCSC's liftOver tool. GWAS datasets were obtained from NHGRI-EBI's GWAS Catalog (https://www.ebi.ac.uk/gwas/home). GWAS sets were selected in three categories - psychiatric disorders (schizophrenia, depression, and ADHD), neurological disorders (Multiple Sclerosis, Alzheimer's), and other conditions that did not involve brain or neuron functions. Only sets that had at least 500 SNPs were selected in order to effectively perform the analysis. SNPs that did not have a reference SNP ID were removed. Only SNPs present in the 1000 Genomes Project Phase 3 European population were kept. For each GWAS set, if there were *n* SNPs in the GWAS set, then *n* SNPs would be randomly selected from all SNPs present in the 1000 Genomes European population set, retaining an identical distribution of SNPs across the chromosomes. The number of differential peaks that overlapped with this SNP test set was calculated and repeated for a total of 10,000 runs (Monte Carlo randomization). From this distribution, we used the R function pnorm, in conjunction with the actual overlap of the GWAS set with the differential peaks, to calculate a p value.

RNA-seq data analysis

Sequencing reads were trimmed under default settings using Trim Galore!. The trimmed reads were mapped to GRCm38 genome by hisat2 (Kim et al., 2015). Mapped bam files were imported into SeqMonk v1.47.1 (Babraham Institute, https://www.bioinformatics.babraham.ac.uk/projects/seqmonk). Datasets with poor quality (percentage of reads aligned to exons < 40%) were discarded. FeatureCounts (Liao et al., 2014) was used to count reads and DEGs were determined by pairwise comparison using DESeq2 (FDR < 0.05). The threshold of FDR < 0.05 was used to be consistent with that used in differential enhancers.

Weighted gene co-expression network analysis

A signed co-expression network was built using the WGCNA package in R (Langfelder and Horvath, 2008). We first normalized gene expression values using log2(FPKM) (Fragments Per Kilobase per Million mapped reads) and then genes were ranked based on their median absolute deviation (MAD). The genes with over 0.3 at MAD were selected as input for the network construction. We converted the normalized gene expression values into an adjacency matrix using the function $a_{ij} = \left|cor(x_i, x_j)\right|^{\beta}$, where x_i and x_j were the expression data of two genes. The value of β was determined to be 7 using the approximate scale-free topology (Zhang and Horvath, 2005). We further performed the topological overlap measure to transform the adjacency matrix into a topological overlap matrix using the blockwiseModules function in the package (with parameters corType = "bicor," TOMType = "signed," minModuleSize = 30, reassignThreshold = 0, mergeCutHeight = 0.15). Modules were then detected based on the topological overlap matrix and the gene expression level of each module was characterized by the module eigengene. The top 100 intramodular hub genes (the most highly connected genes within the module) were identified using the softConnedticity function in the package. The relationship between these hub genes were visualized using Cytoscape (Shannon et al., 2003).

QUANTIFICATION AND STATISTICAL ANALYSIS

All statistical analysis was performed with GraphPad Prism software version 9. Microscope images were taken by an observer who was blind to the experimental conditions. No statistical methods were used to predetermine sample sizes, but our sample sizes are similar to those reported in our previous publications (Ibi et al., 2017). Data distribution was assumed to be normal, but this was not formally tested. Animals were randomly allocated into the different experimental groups. Datapoints were excluded based on previously established criterion and were set to ± 2 s.d. from the group mean. Statistical significance of experiments involving three or more groups and two or more treatments was assessed by two-way ANOVA followed by Sidak's multiple comparison test. Statistical significance of experiments involving time courses and two treatments was assessed by two-way repeated-measures ANOVA. Statistical significance of experiments involving three or more groups was assessed by one-way ANOVA followed by Sidak's multiple comparison test. Statistical significance of experiments involving two groups was assessed by Student's t test. The level of significance was set at p = 0.05. All values in the figure legends represent mean ± s.e.m.

Cell Reports, Volume *37*

Supplemental information

Prolonged epigenomic and synaptic plasticity alterations following single exposure to a psychedelic in mice

Mario de la Fuente Revenga, Bohan Zhu, Christopher A. Guevara, Lynette B. Naler, Justin M. Saunders, Zirui Zhou, Rudy Toneatti, Salvador Sierra, Jennifer T. Wolstenholme, Patrick M. Beardsley, George W. Huntley, Chang Lu, and Javier González-Maeso

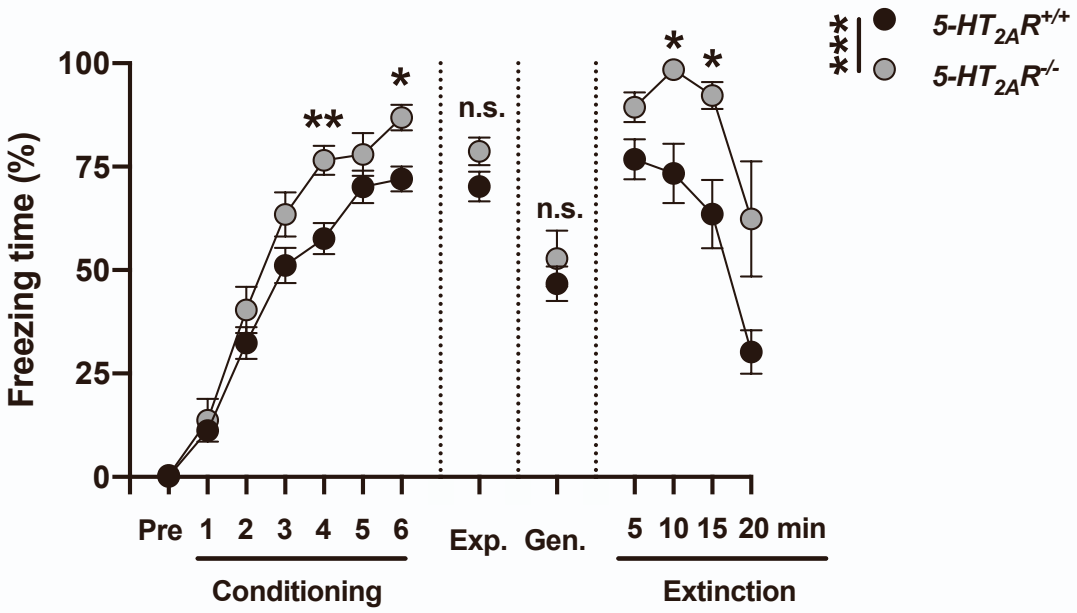

Supplementary Figure S1. Contextual fear extinction in *5-HT$_{2A}$R$^{+/+}$* and *5-HT$_{2A}$R$^{-/-}$* mice (related to Figures 1L and 1J). Fear conditioning (n = 11-26 mice per group; conditioning, $F[6,252] = 118.1$, $p < 0.001$; genotype, $F[1,252] = 18.28$, $p < 0.001$), expression (n = 11-26 mice per group, $t_{36} = 1.46$, $p > 0.05$), generalization (n = 6-15 mice per group, $t_{19} = 0.77$, $p > 0.05$), extinction (n = 6-15 mice per group; extinction, $F[3,76] = 10.34$, $p < 0.001$; genotype, $F[1,76] = 18.69$, $p < 0.001$). Statistical analysis was performed using two-way ANOVA with Sidak's multiple comparison test (conditioning and extinction) or Student's *t* test (expression and generalization). *p < 0.05, **p < 0.01, ***p < 0.001, n.s., not significant. Error bars represent S.E.M.

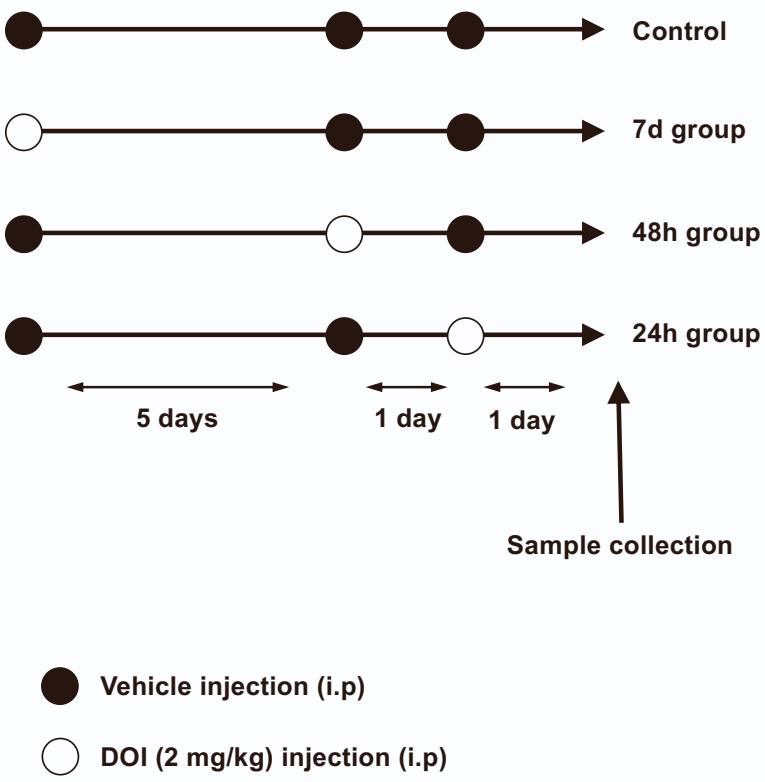

Supplementary Figure S2. Experimental set up of treatment (i.p.) with DOI (2 mg/kg), or vehicle (related to Figures 3 and 4).

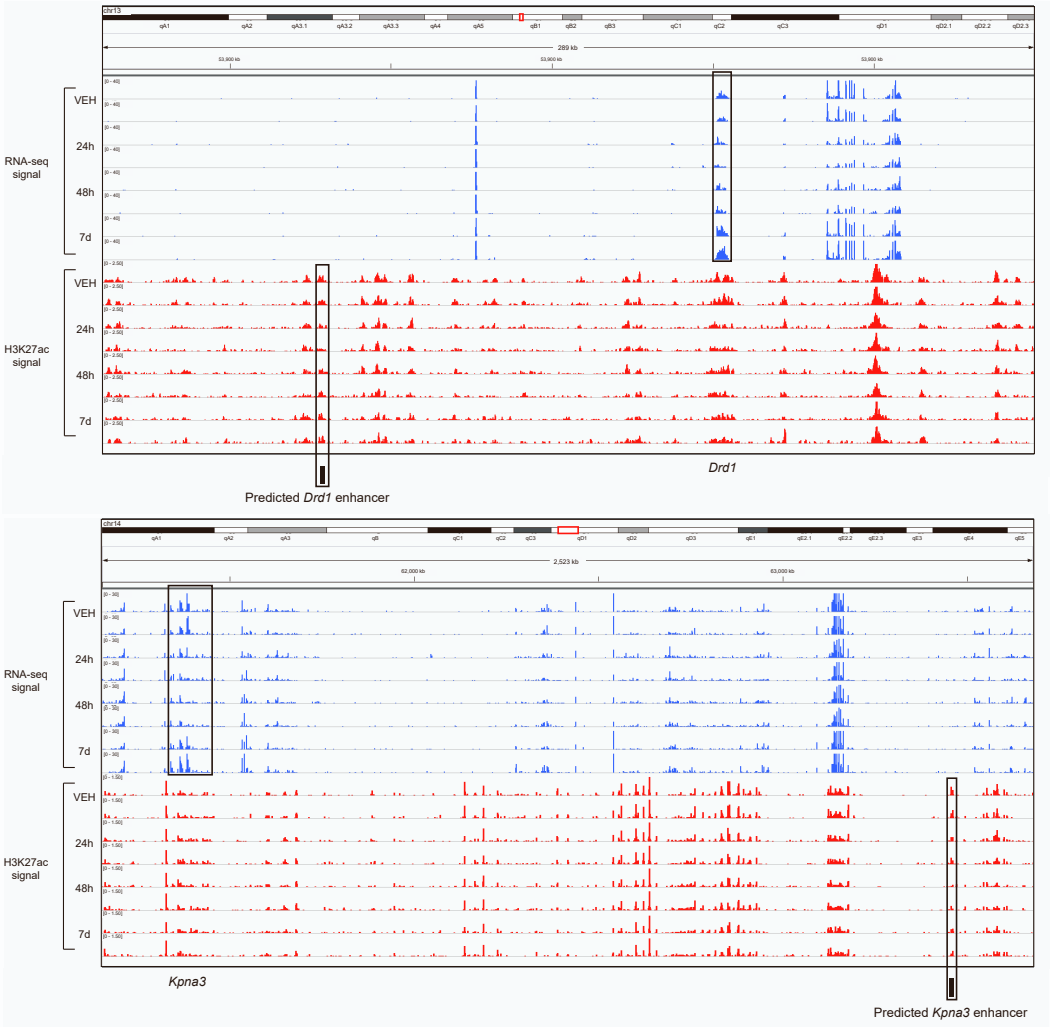

Supplementary Figure S3 (related to Figure 3). Selected genes (*Drd1* and *Kpna3*) with high correlation between enhancer activity and gene expression level. (related to Figures 3 and 4)

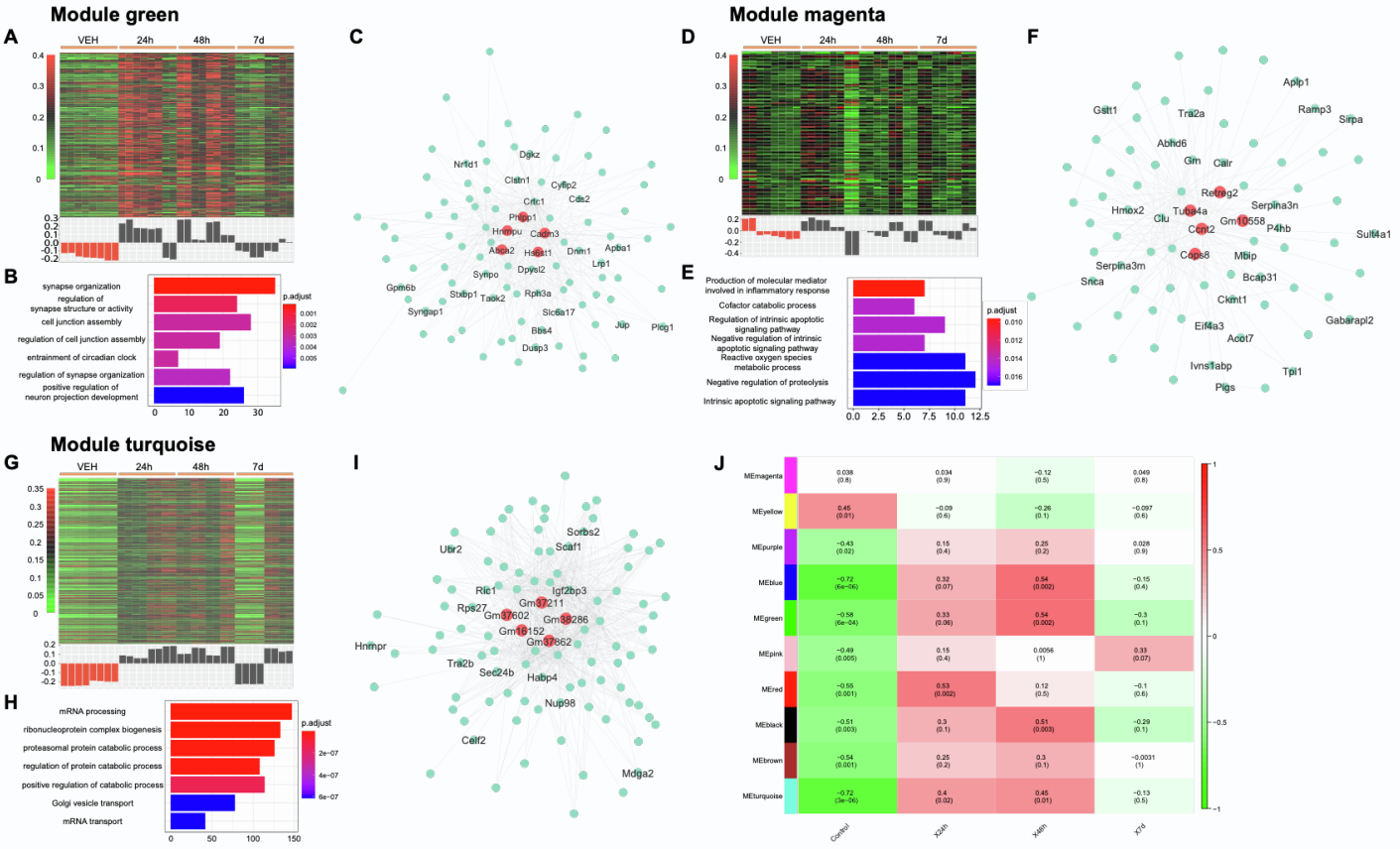

Supplementary Figure S4. Gene co-expression modules (green, magenta, and turquoise) associated with administration of DOI (related to Figure 4**)**

(A,D,G) Heatmap of normalized gene expression profiles in the co-expression module (top). The module eigengene values across samples in four experimental groups (bottom).

(B,E,H) Selected top categories from GO enrichment analysis.

(C,F,I) Visualization of the intramodular connections among the top 100 hub genes in each module. The top 5 genes are in large size and colored orange. The genes involved in the top 15 GO terms are labeled.

(J) Each row corresponds to the module eigengene, column to the status of DOI administration. The two numbers in each cell represented the corresponding correlation coefficient and p value.